Aus der
Eberhard-Karls-Universität Tübingen
Department für Augenheilkunde
Forschungsinstitut für Augenheilkunde, Bereich Neurodegeneration des Auges
Univ.-Prof. Dr. M. W. Seeliger

Einrichtung für Tierschutz, Tierärztlichen Dienst und Labortierkunde
Dr. F. Iglauer

vorgelegt über den
Lehrstuhl für Tierschutz, Verhaltenskunde, Tierhygiene und Tierhaltung
des Veterinärwissenschaftlichen Departments der Tierärztlichen Fakultät
der Ludwig-Maximilians-Universität München
Univ.-Prof. Dr. Dr. M. Erhard

Noninvasive assessment of retinal morphology in mice using optical coherence tomography

Inaugural-Dissertation
zur Erlangung der tiermedizinischen Doktorwürde
der Tierärztlichen Fakultät
der Ludwig-Maximilians-Universität München

von
Gesine Huber
aus Kusterdingen

München 2010

Gedruckt mit der Genehmigung der Tierärztlichen Fakultät

der Ludwig-Maximilians-Universität München

Dekan: Univ.-Prof. Dr. Braun

Referent: Univ.-Prof. Dr. Dr. Erhard

Korreferent: Priv.-Doz. Dr. Deeg

Tag der Promotion: 13.02.2010

Meinem Bruder

Felix

TABLE OF CONTENTS

I. INTRODUCTION

Animal models are important organisms in many areas of science. They play a key role in experimental ophthalmology because they help to understand a variety of genetical, developmental, and disease mechanisms and to develop new pharmaceutical and gene therapies. Especially mice are valuable models to identify the genes involved in vision because of the availability of diverse genetically modified strains and the ease with which single gene mutants can be generated.

The retina as part of the brain offers the opportunity to directly visualize changes associated with neurodegenerative disorders and vascular alterations. There are both morphological and functional approaches to characterize disease phenotypes, to monitor disease progression, and to evaluate the responsiveness to therapy, which can either be performed in living animals (*in vivo*) or in respective ocular tissue (*in vitro*).

Whereas most functional tests, namely electroretinography (ERG), are performed *in vivo*, practically all morphological methods, like histology, are so far performed *in vitro*. The current need to sacrifice animals for histological examinations at different time points interferes with the ability to follow up disease processes and to monitor therapeutic or side effects during the preclinical assessment of novel genetical and pharmaceutical therapy strategies over time in the same individuals.

Optical coherence tomography (OCT) is a novel technique to assess retinal morphology *in vivo*. Commercially available OCTs have been designed for clinical investigations in human ophthalmology. In this work, the establishment of a commercially available OCT for the *in vivo* analysis of mouse models of retinal degenerations is reported.

II. REVIEW

1. Proper use of animals in science

Animal experiments have facilitated numerous advances in fundamental scientific knowledge and most of the benefits of modern medicine. The humane treatment of animals in research is considered important to overcome existing conflicts between demands of science and medicine on one hand, and ethical considerations on the other hand. These considerations resulted in the concept of the three R`s: Replacement, Reduction and Refinement.

1.1 Background

The idea of a more humane treatment of animals used in science was first given serious consideration less than half a century ago (Russel and Burch 1959). Russel and Burch performed a scientific study of humane techniques in laboratory animal experiments. In 1959, they published “The principles of humane experimental technique”, in which they define and explain humane science.

The three R`s are based equally on ethical consideration of animals in the laboratory setting and the recognition that, if the researcher in experimental design and implementation appropriately applies these principles, this results in a situation that is likely to produce more robust scientific results (Goldberg and Locke 2004). The rationale for incorporating the three R`s is commonly neither altruism nor public relations. Rather, methodological improvements are sought as a means to overcome the technical limitations inherent in current animal models. To practicing scientists, these more elegant and relevant methods represent technical progress and are considered to be additional or advanced, rather than alternative methods (Richmond 2002).

1.2 The concept of the three R’s

Animal welfare may be improved by procedures which completely replace the need for animal experiments (replacement), reduce the number of animals required (reduction), or diminish the amount of pain or distress suffered by the animals needed (refinement) (Balls 1983).

1.2.1 Replacement alternatives

Replacement alternatives encompass those methods that permit a given purpose to be achieved without conducting experiments or other scientific procedures on living animals. Russell and Burch (1959) distinguished between relative replacement, e.g. the humane killing of a vertebrate animal to provide cells, tissues, or organs for *in vitro* studies, and absolute replacement in which the use of animals would not be needed at all, e.g. the culture of human invertebrate cells and tissues.

The range of replacement alternative methods and approaches includes improved storage, exchange and use of information about previous animal experiments to avoid unnecessary repetition of animal procedures, use of physical and chemical techniques and predictions based upon the physical and chemical properties in molecules, use of mathematical and computer models, use of organisms with limited sentience such as invertebrates, plants and microorganisms, use of *in vitro* methods including subcellular fractions, tissue slices, cell suspensions and perfused organs, and human studies including use of human volunteers, postmarketing surveillance, and epidemiology. In many areas of biomedical sciences, *in vitro* methods are increasingly used as the methods of choice to replace animal studies because they offer the best scientific approach.

Russell and Burch (1959) warned that the fidelity of mammals as models for man is greatly overestimated; however, replacement alternative methods must be based on good science, and extravagant claims that cannot be substantiated must be avoided.

1.2.2 Reduction alternatives

Reduction alternatives describe methods to obtain comparable levels of information from the use of fewer animals in scientific procedures or to obtain more scientifically valuable information from a given number of animals, for that in the long run, fewer animals are needed to complete a given research project or test.

The number of animals used should be the minimum necessary to test the experimental hypothesis and to give statistically usable results.

1.2.3 Refinement alternatives

Refinement alternatives cover those methods that eliminate or minimize potential pain and distress or enhance animal well-being. Distress is an aversive state in which an animal is unable to adapt completely to stressors and the resulting stress and therefore shows maladaptive behaviour. The stressors may induce physiological,

psychological and environmental stress. Pain results from potential or actual tissue damage, such as that caused by injury, surgery or disease and can lead to distress (Institute for Laboratory Animal Research 1992, Flecknell 1994, Morton and Townsend 1995).

Assessments of animal pain and distress are currently based on subjective evaluation of abnormal behaviour and appearance. Proper evaluation of pain relies largely on the ability to understand the behaviour and needs of each species of laboratory animals. Therefore it is advisable for investigators to assume that a procedure that inflicts pain and distress on humans will inflict pain and distress on animals. To implement the refinement prong of the three R`s it is not enough to simply administer analgesics or anaesthesia to animals in pain. Every procedure in the experimental protocol must be considered from the perspective of the need to reduce or eliminate pain and distress. Thus, noninvasive experiments are finding their way into the laboratory.

1.3 Current guidelines for animal use in science

Current legislation in Europe and the United States mandates the incorporation of the three R`s (Council Directive 86/609/EEC 1986, U.S. Animal Welfare Act). It regulates that all proposed use of laboratory animals should be subject to review to determine whether such use appears to be justifiable both scientifically and ethically. Such laws not only approve Russell`s and Burch`s concept (1959) but place legal and moral obligations on everybody concerned to replace, to reduce and to refine laboratory animal experimentation whenever and wherever possible. Full implementation of this newly developed legislation depends on scientists' ability to understand animal welfare issues and to accept the legitimacy of the publics' interest in the conduct of science.

Within the scientific community, fulfillment of the three R`s paradigm has necessitated a re-evaluation of the extent and manner in which animals are used. Thus, laboratory animal usage proposed for scientific studies now warrants prior consideration of factors such as relevance, ethical concerns, potential benefits, and scientific justification. Furthermore, legal and moral accountability to the principles of the three R`s has compelled consideration of alternative methods that have the potential to achieve replacement, reduction and refinement of laboratory animal experimentation.

There is a general agreement that the best animal welfare results in the best science.

Thus, “alternative” methods enabling reduction, refinement and/ or replacement are in reality often more scientifically “advanced” and valid methods (Richmond 2002).

1.4 Current guidelines for animal use in eye research (ARVO)

All experiments in ophthalmological research including those presented in this work were performed according to the “Statement for the Use of Animals in Ophthalmic and Visual Research” of the **A**ssociation for **R**esearch in **V**ision and **O**phthalmology (ARVO).

The fundamental principle of the ARVO statement is that animals must not be subjected to avoidable distress or discomfort. The investigator's first concern must therefore be to avoid the use of animals whenever possible.

Nevertheless, the work with living animals is essential to continued progress in many areas of clinical and basic research on vision, because its aim is to understand the structure and function of complex and intricately connected biological systems. Therefore, the proper use of animals in research contributes honorably and essentially to the improvement of human and animal lives.

ARVO provides guidelines intended for the investigator responsible for the humane care and use of animals in vision research, because the concern for the humane treatment of animals obliges to establish that the potential benefits to human and animal health outweigh the cost in animal lives (ARVO 2009).

2. The visual system

The visual system as part of the central nervous system enables organisms to see. Vision originates in the photoreceptors of the retina, a layer of cells at the back of the eye. This information is then processed by a network of horizontal, bipolar and amacrine cells. Ganglion cells further process these signals and send the information to the brain via the optic nerve, which consists of their axons. The optic nerves of both eyes meet and partially cross at the optic chiasm at the base of the hypothalamus. At this point the information coming from both eyes is combined and then splits according to the visual field in a right and left optic tract. The optic tract wraps around the midbrain and reaches the lateral geniculate nucleus (LGN), where all the axons form synapses. The LGN is a sensory relay nucleus in the thalamus, whose neurons form the optic radiation and pass the visual information on to the primary visual cortex. The visual cortex is responsible for processing the visual image. It is located at the posterior end of the brain above the cerebellum.

2.1 Anatomy of the eye

The eyes of all vertebrate animals are constructed upon a common architectural plan (Rodieck 1998). They are composed of three concentric tunics or layers (1-sclera and cornea; 2-iris, ciliary body and choroid; 3-retina) and three chambers of fluid (anterior chamber, posterior chamber; vitreous) (Detwiler 1955) (Fig.1).

The external layer (1), which includes the sclera and cornea, is designed for protection and also for the entrance and refraction of light. The cornea is a transparent external surface which covers both pupil and iris. It merges into the sclera, which is part of the supporting wall of the eyeball and is in continuity with the dura of the central nervous system.

The anterior chamber, placed between cornea and iris, is filled with aqueous humor.

The intermediate layer (2) is divided into two parts. The anterior part consists of iris and ciliary body, and the posterior part of the highly vascular and thus nutritive choroid. The iris is a disc-shaped pigmented contractile membrane whose degree of pigmentation is responsible for the eye color. It is attached at its margin to the ciliary body and has a central opening, the pupil. The ciliary body is the part of the eye between the choroid and the iris to which the ciliary muscle is attached. It is also highly vascularized and controls the intraocular pressure by the amount of aqueous humor released into the posterior chamber by ultrafiltration. The choroid is located between retina and sclera. It is composed of layers of blood vessels that nourish the

back of the eye.

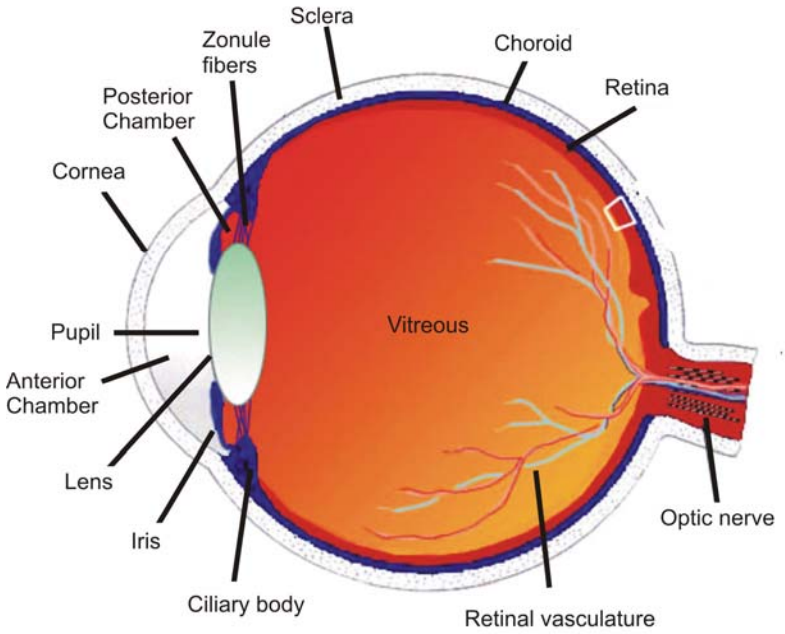

Fig. 1: Morphology of the eye (modified from Heckenlively and Arden 2006).

The posterior chamber is situated between iris, zonule fibers and lens, and is connected to the anterior chamber via the pupil.

The lens, which focuses light rays on the retina, is located between iris and vitreous. A normal lens contains about 65% water and 35% protein (Spalton et al. 1994). The lens is suspended by zonule fibers attached to the anterior portion of the ciliary body. These fibers translate any increase or reduction in the tone of the ciliary muscle into shape changes of the lens, a process called accommodation that allows to form sharp retinal images of objects at different distances.

The vitreous is located between lens and retina. It is filled with vitreous humor, which is a jelly-like substance supporting the structure of the eye. Besides, it maintains the transparency of the eye because it is impervious to debris.

The retina (3) is an outpouching of the central nervous system (CNS) that covers the back wall of the eye (Rattner et al. 1999). It is inverted, i.e. the receptor elements are turned away rather than towards the source of illumination (Detwiler 1955). Light must, therefore, travel all the way through the retina before it reaches and activates the photosensitive part of the photoreceptor cells.

2.2 Retinal structure

The retina is part of the brain and has essentially a horizontally layered structure, consisting of several cell types. The different retinal layers are usually subdivided into an inner and an outer part.

2.2.1 Overview of the retinal layers (Fig. 2)

a the retinal pigment epithelium (RPE)

b the outer and inner segments (OS/IS) of photoreceptor cells (1,2)

c the outer limiting membrane (OLM), a narrow zone of junctions between Müller cells and the ciliar region of photoreceptor outer segments

d the outer nuclear layer (ONL), representing photoreceptor cell bodies

e the outer plexiform layer (OPL), formed by processes involved in the synaptic connection between photoreceptor (1,2), bipolar (4), and horizontal cells (3)

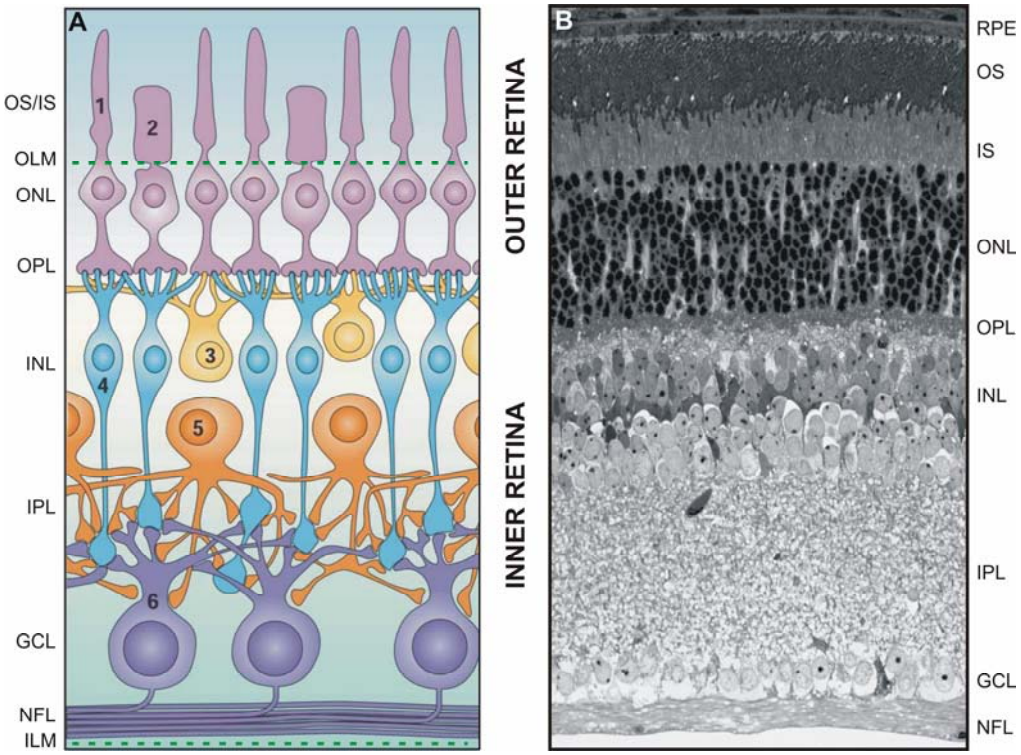

Fig. 2: Retinal Structure. (A) Functional organization of the vertebrate retina (modified from Wässle 2004). (B) Histology of a murine retina (kindly provided by C. Grimm, Zurich, Switzerland). (1) Rods, (2) Cones, (3) Horizontal cells, (4) Bipolar cells, (5) Amacrine cells, (6) Ganglion cells. RPE: Retinal Pigment Epithelium, OS/IS: Outer/Inner Segment, OLM: Outer Limiting Membrane, ONL: Outer Nuclear Layer, OPL: Outer Plexiform Layer, INL: Inner Nuclear Layer, IPL: Inner Plexiform Layer, GCL: Ganglion Cell Layer, NFL: Nerve Fiber Layer, ILM: Inner Limiting Membrane.

f the inner nuclear layer (INL), representing cell bodies of horizontal (3), bipolar (4) and amacrine cells (5) and the nuclei of Müller cells

g the inner plexiform layer (IPL), formed by processes involved in synaptic connections between bipolar (4), amacrine (5), and ganglion cells (6)

h the ganglion cell layer (GCL), containing cell bodies of ganglion (6) and “displaced” amacrine cells

i the nerve fiber layer (NFL), formed by the axons of ganglion cells

k the inner limiting membrane (ILM), representing the endfeet of Müller cells

2.2.2 Outer retina

The outer retina consists of four different layers: the retinal pigment epithelium, the photoreceptor outer and inner segments, the outer nuclear layer, and the outer plexiform layer (Fig. 2).

The retinal pigment epithelium (RPE) is a highly pigmented monolayer (Martinez-Morales et al. 2004), which is located between the photoreceptors and the choroid (Fig. 1). It is an important part of the blood-retina barrier, maintains adhesion, and controls the transport of ions, water, retinol, and other metabolites between retina and choroid. Furthermore, it improves the quality of vision by absorbing stray light in melanin granules, thus preventing the degradation of the visual image. An important function is also the phagocytosis of remnants of photoreceptor outer segments, which are constantly renewed, and the protection against free radicals (Bok 1993, Boulton and Dayhaw-Barker 2001, Futter et al. 2004).

On the choroidal side, the RPE is firmly attached to Bruch's membrane. Both RPE and the choroid contribute to elements of this membrane, which consists of five layers and reaches from the optic disc to the "ora serrata" where the retina ends anteriorly. The innermost layer of Bruch's membrane is formed by the basement membrane of the RPE cells. This is followed by an inner collagenous zone, an elastic layer, an outer collagenous zone, and finally the basement membrane of the choroid (choriocapillaris).

The photoreceptors and their connections form the photoreceptor outer and inner segment layer (OS/IS), the outer limiting membrane (OLM), and the outer nuclear layer (ONL), which consists of the cell bodies of the photoreceptors. The synaptic terminals also contribute the outer plexiform layer (OPL). Photoreceptor cells are highly specialized to convert light into nerve signals. Their distal parts (inner and outer segments) are optimized for capturing light, and their proximal parts to synapse the information to the inner retina. The two main classes of photoreceptor cells are the light-sensitive rods that facilitate vision at low light levels, and the less sensitive cones working best under daylight conditions and permitting color vision.

Rods are so extremely sensitive that they are capable of recognizing a single photon, and thus are used for vision in very dim environments or at night (scotopic vision). They contain the visual pigment rhodopsin, which is sensitive to blue-green light with a maximum at a wavelength of about 500 nm (Detwiler 1943).

Mammals usually feature one type of rods but two or three types of cones. Primates commonly exhibit red, green, and blue cones that are maximally sensitive to light with

either long wavelengths (red, 588 nm), medium wavelengths (green, 531 nm) or short wavelengths (blue, 429 nm) (Curcio et al. 1987). Most other mammals including rodents typically exhibit only short wavelength-sensitive (SWS) cones, equivalent to blue cones, and medium wavelength-sensitive (MWS) cones, corresponding to green cones, but no red cones. The spectral sensitivity is determined by the molecular structure of their visual pigments, the cone opsins.

Photoreceptor cells consist of a cell body, an outer and an inner segment, and synaptic terminals (Kaneko 1979) (Fig. 3). The outer segments, the light sensitive parts of the photoreceptors, are connected to the inner segments by a narrow connecting stalk, which includes a cilium arising from a basal body in the inner segment. With the exception of some diurnal mammals, rod cell bodies form the majority of the outer nuclear layer.

Cones are usually shorter and thicker than the long, slim rods. Their cell bodies are commonly situated in the distal part of the outer nuclear layer (ONL), and their outer segments in the region of the rod inner segments.

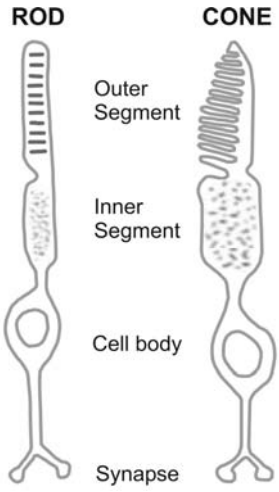

Fig. 3: Sketch of rod (left) and cone (right) photoreceptor structure (modified from Kellner und Wachtlin 2008).

Apical processes from the retinal pigment epithelium are in contact with the outer segments of both rods and cones. This is important as the outer segments have to be constantly renewed. In rods, outer segment renewal involves the synthesis of disc material in the inner segments and the formation of new discs in the region of the cilium at the rate of about one to five per hour. The used discs are discarded of by intermittent shedding of the tips of the photoreceptor outer segments depending on

the circadian rhythm (i.e. during subjective night). The debris is then finally phagocytosed by the RPE. In rods, the entire outer segment is replaced every 8-14 days, and in cones, a complete renewal takes about 9 months to one year (Rodieck 1998).

The outer plexiform layer (OPL) includes synaptic bodies of photoreceptor synapses with bipolar and horizontal cells (rod spherules and cone pedicles, respectively), the dendrites of bipolar and horizontal cells, and Müller cell processes. The outer limiting membrane (OLM) of the retina is an alignment of adherent junctions between Müller cells and photoreceptor cell inner segments (Bunt-Milam et al. 1985). Müller cells extend beyond the outer limiting membrane into the subretinal space where they form microvilli. Their surface is increased so they can more easily exchange metabolites and ions with the subretinal space. The OLM forms a barrier between the subretinal space and the more proximal neural retina.

2.2.3 Inner retina

The inner retina further processes and reduces the visual information and facilitates the transfer towards the more central brain areas. It consists of four different layers: the inner nuclear layer (INL), the inner plexiform layer (IPL), the ganglion cell layer (GCL), and the nerve fiber layer (NFL) (Fig. 2).

The inner nuclear layer (INL) contains the cell bodies of four types of cells: horizontal cells, bipolar cells, amacrine cells, and Müller cells.

Horizontal cells are believed to be involved in contrast vision. They process information from groups of photoreceptors and provide local feedback in the outer plexiform layer. Bipolar cells collect and process information from the outer retina and relay it to the amacrine and/or ganglion cells in the proximal inner retina. The inner plexiform layer (IPL) is an ordered stack of synaptic planes where bipolar cells branch at different levels (Cajal 1972).

Some bipolar cells also form synapses with certain amacrine cells in the IPL, which modify or even transmit the signal to ganglion cells. Most amacrine cells are located in the proximal part of the inner nuclear layer, but some can be found in the ganglion cell layer or even in the NFL (“displaced” amacrine cells). As far as it is known, they all modulate signals in the inner plexiform layer but are diverse in both their morphology and neurochemistry (Kolb et al. 2002).

Müller cells are the main glial cells which also form the scaffold of the retina. They extend through the entire retina, but their nuclei are located in the inner nuclear layer. In both inner and outer plexiform layer, Müller cell processes cover the dendritic

processes of the neurons to the synaptic clefts. In the nerve fiber layer, the Müller cell processes cover most ganglion cell axons (Ogden 1983). Apart from supporting the retinal structure, Müller cells seem to be associated with nutrition of the photoreceptor inner segments and the generation of neuronal impulses. They act as ionic reservoir during hyperpolarization of the photoreceptor upon light stimulation. They also form the major element of scar tissue, or gliosis, which is the retina's characteristic response to cell death or disease (Spalton et al. 1994).

The ganglion cell layer (GCL) consists of ganglion and the aforementioned "displaced" amacrine cells. Ganglion cells are neurons that collect all visual information processed in the retina and pass it on to the brain via the optic nerve (Fig. 1). Their cell bodies are located mainly in the ganglion cell layer, and their dendrites form synapses with bipolar and amacrine cells which are located in the inner plexiform layer (Wässle 2004).

The nerve fiber layer (NFL) is located closest to the vitreous, and is formed by axons of ganglion cells as they converge from all parts of the retina toward the optic disc. The ganglion cell axons form small bundles in the NFL; these bundles are often surrounded by glial cell processes of Müller cells or astrocytes.

In different layers, components of the Müller cells form the so-called "limiting membranes". The proximal end of the Müller cells terminate in an expansion (endfoot), which rests on its basal lamina, called the inner limiting membrane (ILM). The ILM is the inner surface of the retina bordering the vitreous and thereby forming a diffusion barrier between neural retina and vitreous humor.

2.2.4 Retinal vasculature

The ocular blood supply has external and internal components. The entire outer retina is free of vessels and receives its support exclusively from the choroid and the choriocapillaris, mediated by the RPE. The inner retina gets its supply from intraocular vessels entering the eye together with the optic nerve (Fig. 1).

These central retinal vessels divide into several main branches shortly after their entry at the optic disc (Fig. 4A, C, D), and then further subdivide in several steps down to the capillary level. In rodents, three major capillary beds of the retinal circulation are present (Cuthbertson and Mandel 1986), a proximal one at the level of the nerve fiber layer, an intermediate one at the junction of inner plexiform and inner nuclear layer, and a deep one at the outer plexiform layer (Fig. 4B) . In mice, retinal vessels develop gradually after birth in a radial fashion starting at the optic disc. At

the time of eye opening after about two weeks, they reach the retinal periphery (Michaelson 1948, Connolly et al. 1988).

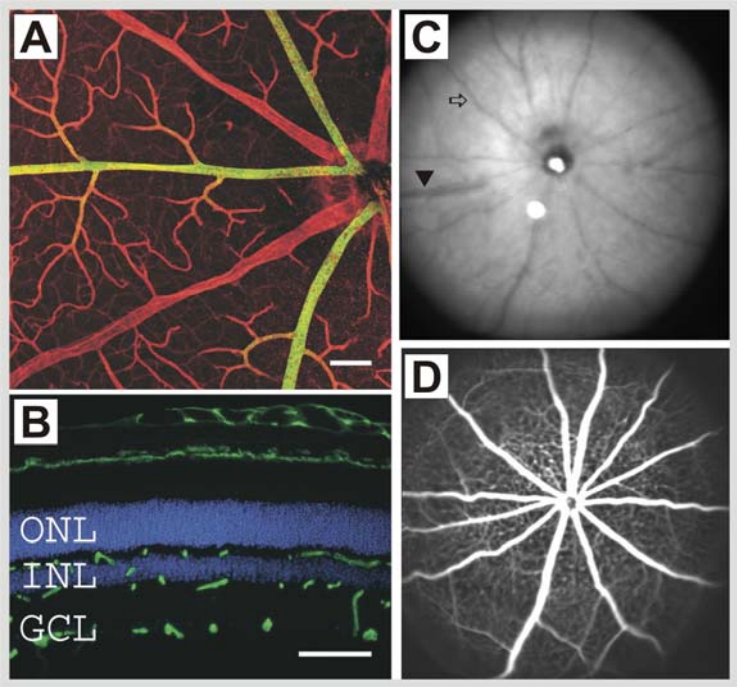

Fig. 4: Retinal vasculature in mice. (A) Retinal flat mount immunostained with anti-smooth muscle actin (green) to visualize arteries and arterioles, and with anti-collagen IV (red) to label the perivascular basement membrane. (B) Fresh-frozen retinal cross-section immunostained with anti-collagen IV (green) to visualize vessels, and DAPI (blue) to mark outer and inner nuclear layers. ONL: Outer nuclear layer, INL: Inner nuclear layer, GCL: Ganglion cell layer. (C) Native SLO imaging of retinal (arrow) and choroidal (arrowhead) vasculature (D) Fluorescein angiography of retinal vasculature. Panels (A) and (B) are taken from Xu et al. 2004, (C) and (D) are own data.

The outer retina is supplied by the choroid (choriocapillaris) located beneath the RPE. To accommodate visual function, the outer retina is completely avascular and receives its metabolic supply from the choroidal circulation by active transport through the RPE. Together, active transport mechanisms and tight junctions, which prevent free diffusion, constitute the outer blood-retinal barrier, a mechanism whereby photoreceptors are only exposed to selected molecules (Spalton et al. 1994).

3. RETINAL IMAGING

The optical apparatus of the eye designed to project an image may also be used to visualize retinal structures without the need for any manipulation. It is the only place in the body where blood vessels of the microvascular level are visible noninvasively (Liew et al. 2008). Retinal imaging is thus helpful to make predictions about the vascular status of other parts of the central nervous system and the cardiovascular system in general (Sharma and Ehinger 2003). The application of dyes in angiography allows an even more specific assessment of the vasculature.

Whereas conventional imaging with a fundus camera becomes difficult to impossible with decreasing pupil size, recent imaging techniques based on narrow laser beams such as scanning laser ophthalmoscopy and optical coherence tomography are well suited to assess retinal morphology even in the small eyes of rodents.

3.1 Scanning laser ophthalmoscopy

Scanning laser ophthalmoscopy (SLO) is a diagnostic technique for confocal imaging of the eye with a narrow laser beam *in vivo* (Fig. 5). Although it does not provide color images like a conventional fundus camera, the low beam width and the confocal diaphragm make it particularly attractive for the examination of small animal models.

The use of lasers of different wavelengths allows obtaining information about specific tissues and layers due to their transmission characteristics. Laser light of shorter wavelengths (blue-green) is generally more strongly absorbed by ocular structures – especially melanin granules in the retinal pigment epithelium (RPE) and choroid – than that of longer wavelengths (near infrared) (Preece and Claridge 2002). Consequently, the short wavelength lasers provide higher contrast images of the retina but are unable to penetrate the RPE/choroid in pigmented animals, whereas the infrared lasers give less retinal details but can pass through the choroid down to the sclera (Fig. 5B). The comparison of images taken with the different wavelengths provides information about specific tissues and layers due to their reflection and transmission characteristics. In addition, fluorescent dyes excitable in the blue and infrared range offer a unique access to the vascular structures associated with the eye (Seeliger et al. 2005).

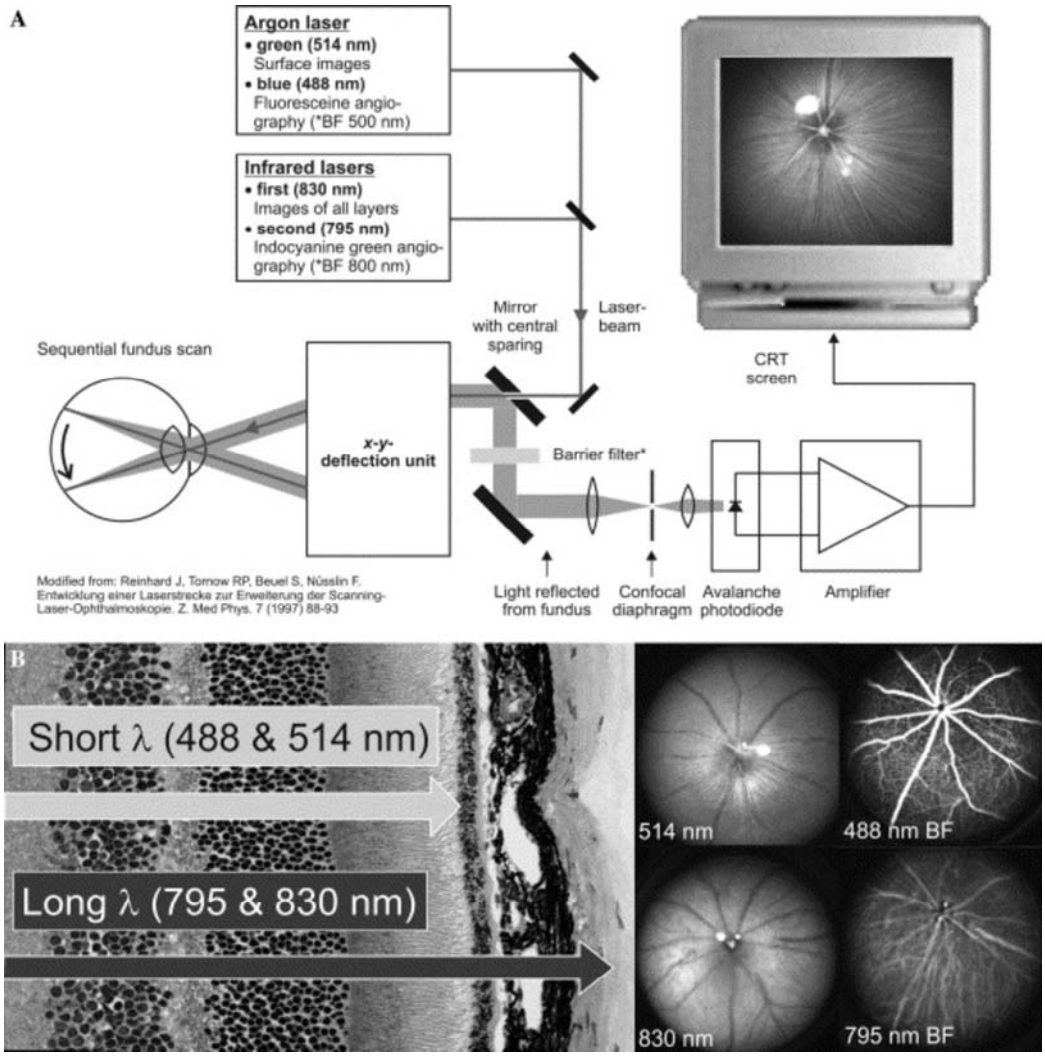

Fig. 5: Technical overview of scanning laser ophthalmoscopy (SLO) (Seeliger et al. 2005). (A) Image generation in a confocal SLO system. (B) Layer selectivity of the different laser wavelengths.

3.2 Optical coherence tomography

Optical coherence tomography (OCT) provides high-resolution, micron-scale, cross-sectional or tomographic images of the internal microstructure in biological tissues (Huang et al. 1991a, Izatt et al. 1994, Hee et al. 1995, Fujimoto et al. 2000, Fujimoto 2003, Drexler et al. 2001). The results are similar in appearance to ultrasonographic scans. Instead of sound, OCT uses laser light to obtain a reflectivity profile of the tissue under investigation (Huang et al. 1991a), which provides greater resolution (Li et al. 2001). The main difference between ultrasound and optical imaging is that the velocity of light is almost a million times faster than the velocity of sound. Another advantage, compared to ultrasound, is that OCT requires no contact medium, as the optical impedance, which is the refractive index between air and tissue, is not as large as the difference in acoustic impedance between air and tissue. Therefore it is not only noninvasive but also noncontact, which has some advantages with respect to hygiene. As long as the light exposure is limited to a certain level and duration, it is also safe for the patient examined (Wojtkowski et al. 2004).

3.2.1 Technical principle of optical coherence tomography

The original time-domain OCT (TD-OCT) is frequently compared to ultrasound because of their analogous basic principles. Both methods create a cross-sectional image by measuring the echo time delay and intensity of the reflected and backscattered light or sound. The velocity of light is much faster than that of sound, therefore OCT uses low-coherence interferometry to measure the time delays between reflections from different layers (Born et al. 1999). In conventional TD-OCT (Fig. 6), the low-coherent laser beam is divided into two parts by a partially reflecting mirror (beamsplitter). One part of the light beam is directed onto the sample under examination and is reflected from sample structures at different distances. The other one is directed to the reference arm inside the device with a mirror at a variable, known spatial position. The reflected reference beam travels back to the beamsplitter where it is combined with the beam reflected from structures within the eye.

Time-domain systems use a moving reference mirror for measuring the return time of the light from the retina (Fig. 6). This mechanical moving reference mirror limits the speed at which data is acquired. Since it works on the “time of flight” principle, it is known as “time-domain” OCT (TD-OCT).

In order to measure reflectivity at a given depth within the eye, the reference mirror has to be in the corresponding location (Huang et al. 1991a, Fercher et al. 1993).

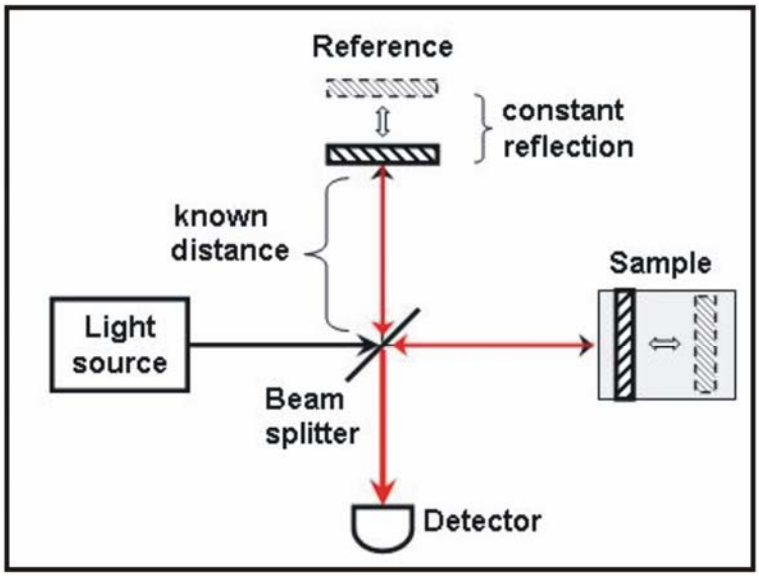

Fig. 6: Principle of conventional time-domain OCT with moving reference mirror.

The combination of the reference beam with the signal from the sample arm then provides information about the tissue reflectivity at the chosen depth. To obtain reflectance information for the entire light path within the sample, the position of the reference mirror may be varied continuously. If there are reflecting structures at different depths of the sample, then there will be a signal peak observed each time the delay of the reference beam matches the respective depth. Thus, it is possible to perform high-resolution measurements of the thickness of different structures (Fercher et al. 1988, Huang et al. 1991b, Hitzenberger 1992, Swanson et al. 1992). The light source, a compact superluminescent diode, usually emits continuous light waves having a short or low coherence length.

The technical principle of spectral domain optical coherence tomography (SD-OCT) (see 3.2.3) is similar, however, the signal acquisition varies importantly. SD-OCT acquires all information in one single axial scan simultaneously by evaluating the frequency spectrum of the interference between the reflected light and a stationary reference mirror (Fig. 7). Therefore, the interference pattern is decoded and split into its frequency components by a Fourier transformation. Each detected frequency corresponds to a certain depth within the tissue, and all of these components are simultaneously detected. The use of broadband light sources instead of low-coherent ones enables a higher depth resolution (Drexler et al. 2001). Thus, SD-OCT currently outmatches TD-OCT as it combines high resolution with high recording speed (de Boer et al. 2003, Leitgeb et al. 2003, Nassif et al. 2004, Cense et al. 2004, Wojtkowski et al. 2004, Kim et al. 2008).

3.2.2 Development of OCT imaging

Since its introduction in the early 1990s, optical coherence tomography has become a powerful method for imaging the internal structure of biological systems and materials. OCT is ideally suited for ophthalmological purposes because of the ease of optical access to the eye. Ocular media are essentially transparent, they transmit light with only minimal optical attenuation and scattering and provide easy optical access to the retina. For those reasons, ophthalmic diagnosis is the most clinically developed OCT application (Hee et al.1995, 1998, Massin et al. 2000, Puliafito et al. 1995, Schumann et al. 1995, 1996, 2004).

In vitro application of OCT for retinal imaging was initially reported in 1991, illustrating microstructural alterations of the tomographic architecture in vertical sections of the retina (Huang et al. 1991a,b).

The first *in vivo* OCT imaging studies of the human retina were performed in 1993 (Fercher et al. 1993, Swanson et al. 1993). Since that time, OCT has rapidly made its way as a noninvasive, optical medical diagnostic imaging modality that enables *in vivo* cross-sectional visualization of the internal microstructure in biological systems (Fercher et al. 1995, Fujimoto 2003, Fujimoto et al. 1995). OCT provides images of retinal structure that cannot be obtained by any other noninvasive diagnostic technique. Within a few years, the possibility of *in vivo* imaging of both healthy and pathologic retina and in particular the ease with which these images can be acquired considerably changed the diagnostic strategy used by ophthalmologists (Hee et al. 1995, 1996).

Podoleanu et al. (1997, 1998) pioneered the development of a different approach to OCT imaging. This method involves en-face scanning in the XY plane, and combines high-resolution tomographic images with the surface imaging capability of the scanning laser ophthalmoscope (SLO) (see 3.1). The combination of SLO and OCT offers the possibility to combine en face and cross-sectional images to provide complementary information. Indeed, en face images can reveal structures that pass unseen in cross-section and *vice versa*.

Commercial OCT is one of the new standards for *in vivo* noninvasive ophthalmic imaging and is widely used for diagnosis and treatment monitoring of various ocular diseases in humans (Ruggeri et al. 2007). Several companies have commercialized stand-alone units and a third generation system from Heidelberg Engineering (Heidelberg, Germany) combining spectral-domain OCT (SD-OCT) with angiography recently became commercially available (Rosen et al. 2009).

3.2.3 Third generation spectral domain optical coherence tomography

In the present work, high-resolution *in vivo* imaging was carried out with a novel third generation instrument (Spectralis HRA+OCT®, Heidelberg Engineering, Heidelberg, Germany) (Fig. 8A) which allows simultaneous recording of confocal scanning laser ophthalmoscopy (cSLO) and spectral-domain optical coherence tomography (SD-OCT) (Helb et al. in press).

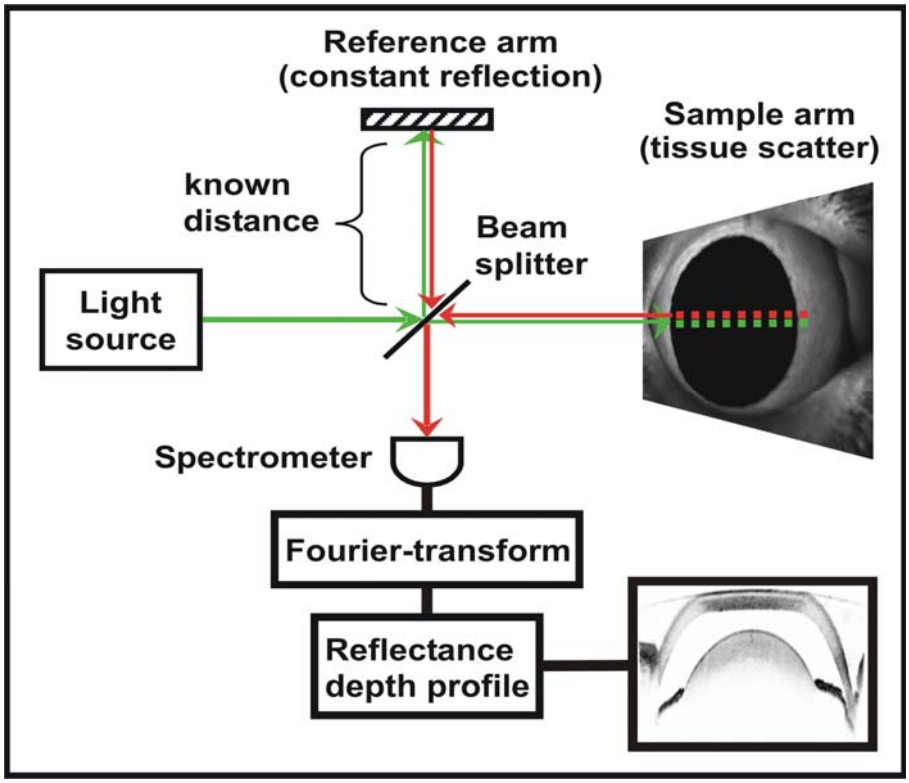

Fig. 7: Technical principle of a third generation spectral domain OCT (Fischer et al. 2009).

Different laser wavelengths allow obtaining information about specific tissues and layers due to their reflection and transmission characteristics. Furthermore, fluorescent dyes excitable in the blue and infrared range offer a unique access to the vascular structures associated with each layer.

The Spectralis HRA+OCT® used in this work offers six imaging modalities to assess the eye:

(1) Infrared (IR)

Infrared light (820 nm) is used to image both retinal and choroidal structures. Laser light of longer wavelengths gives less retinal details but is able to penetrate the RPE/choroid in pigmented retinas.

(2) Red-free (RF)

Laser light of shorter wavelengths is generally more strongly absorbed by ocular structures - especially melanin granules in the retinal pigment epithelium (RPE) and choroid (Preece and Claridge, 2002). Consequently, the short wavelength lasers provide higher contrast images of the retina but cannot penetrate the RPE/choroid in pigmented retinas. It is thus used for fundus imaging, especially for the nerve fiber layer and large retinal vessels, i.e. arteries and veins.

(3) Autofluorescence (AF)

The 488 nm wavelength is used for fundus autofluorescence (FAF) analyses, which reveals the presence of natural fluorophores in the retina and the RPE.

(4) Fluorescein Angiography (FLA)

Fluorescein is a dye that emits light at 400 nm and above when excited at a wavelength of 488 nm. To allow only the light emitted by the dye upon stimulation to become visible, a barrier filter at 500 nm is used to remove the light associated with the excitation. Thus, only the vessels that carry the dye remain to be seen. FLA provides the most detailed images of retinal capillaries.

(5) Indocyanine Green Angiography (ICGA)

Indocyanine green (ICG) is a dye that emits light at 800 nm and above when excited at a wavelength of 795 nm. Similar to FLA, a barrier filter at 800 nm is used to remove the light associated with the excitation. The main difference is a stronger bond of ICG to plasma proteins, and the advantages of longer wavelengths to provide information about choroidal vessels (Seeliger et al. 2005).

(6) Spectral-domain OCT (SD-OCT)

The Spectralis HRA+OCT® device scans the retina at 40.000 A-scans per second, which is a hundred times faster than time-domain OCT. A broadband light source is used to simultaneously measure multiple wavelengths across a spectrum, hence the name “spectral-domain” (also known as Fourier-domain OCT).

Since SD-OCT has extremely high-resolution, it is essential to compensate for eye motion during the image acquisition because it causes image blurring. Therefore the manufacturers use the cSLO technology to track the eye and to guide the OCT to the selected location (TruTrack™). Because of two independent pairs of scanning mirrors, eye movements are registered and automatically corrected, allowing for pixel-to-pixel correlation of cSLO and OCT findings. TruTrack™ is an automatic retinal recognition technology which enables follow-up examinations to be scanned in the same exact location without relying on the operator to pick the spot.

Besides the advantages of SD-OCT mentioned so far, Spectralis HRA+OCT® is the only instrument to center the SD-OCT wavelength at 870 nm. Therefore, it has better light penetrating properties than other systems using shorter wavelength light (820 nm). Also, the longer wavelength has the advantage of opening up the optical window for compatibility with the many other wavelengths used by the set-up (Heidelberg Engineering 2009).

3.2.4 OCT in animal eye research

Retinal morphology has been assessed noninvasively using techniques such as optical coherence tomography (OCT) and scanning laser ophthalmoscopy (SLO) in animal models of retinal degenerative diseases, namely rodents and dogs (Farber et al. 1994, Hauswirth and Timmers 2000, Panzan et al. 2004, Grieve et al. 2005, Lhériteau et al. 2009). OCT has also been used to study retinal microanatomy in chicken (Huang et al. 1998).

The basic feasibility of obtaining OCT images of the mouse retina has been demonstrated in 2001 (Li et al. 2001, Horio et al. 2001, Ko et al. 2004), but acquiring

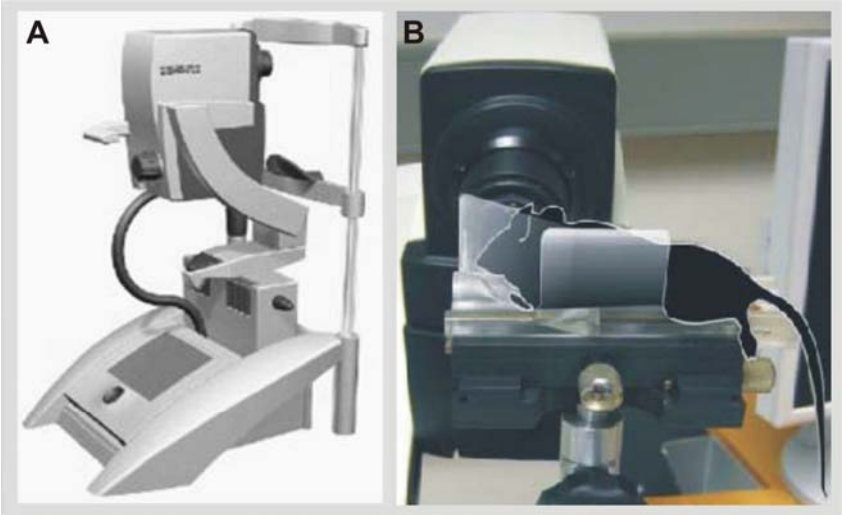

Fig 8: (A) Heidelberg Engineering Spectralis HRA+OCT® used in this work. (B) OCT setup for imaging in mice.

images of the mouse *in vivo* has been a time consuming challenge. (Xu et al. 2002, Paques et al. 2006, Ruether et al. 1997). Horio and Li used a custom-made time-domain OCT (TD-OCT) to study mouse models of retinal degeneration. TD-OCT was able to resolve thinning of the mouse retina, but the low depth resolution of the used systems precluded resolution of detailed retinal microstructures.

There are several challenges in developing a retinal imaging system suitable for routine *in vivo* quantitative morphologic evaluation in small animals. It is difficult to align the mouse eye with the optical system due to the small size of the pupil, the large refractive power of the mouse eye and the lack of voluntary fixation (Kocaoglu et al. 2007). The small pupil size of the mouse eye makes the alignment for light delivery to the eye difficult. It also limits the beam size and thus the amount of light reflected from the retina, which decreases the signal-to-noise ratio.

Although several groups have overcome technical challenges and were able to perform OCT imaging of retinas in small animals including mice (Ko et al. 2004, Kim et al. 2006), the reported self-made systems have limitations. Most lack the depth resolution and the image quality to resolve subretinal layers, therefore, the systems are not suitable for automatic quantitative retinal analysis. Moreover, custom-made setups interfere with the request for standardized examination protocols and thus the comparability of results.

Therefore, the adaptation and establishment of a commercially available third generation OCT device designed for human use was assessed for imaging of the murine retina in this work.

III. MANUSCRIPT

PLoS ONE

First published on Oct 19th, 2009 as doi:10.1371/journal.pone.0007507

Noninvasive *in vivo* assessment of mouse retinal structure using optical coherence tomography

M. Dominik Fischer, Gesine Huber, Susanne C. Beck, Naoyuki Tanimoto, Regine Muehlfriedel, Edda Fahl, Christian Grimm, Andreas Wenzel, Charlotte E. Remé, Serge A. van de Pavert, Jan Wijnholds, Marek Pacal, Rod Bremner, and Mathias W. Seeliger

OPEN ACCESS Freely available online

PLoS one

Noninvasive, *In Vivo* Assessment of Mouse Retinal Structure Using Optical Coherence Tomography

M. Dominik Fischer[1☯], Gesine Huber[1,2☯], Susanne C. Beck[1], Naoyuki Tanimoto[1], Regine Muehlfriedel[1], Edda Fahl[1], Christian Grimm[3], Andreas Wenzel[3¤a], Charlotte E. Remé[3], Serge A. van de Pavert[4¤b], Jan Wijnholds[4], Marek Pacal[5], Rod Bremner[5], Mathias W. Seeliger[1]*

1 Division of Ocular Neurodegeneration, Centre for Ophthalmology, Institute for Ophthalmic Research, University of Tuebingen, Tuebingen, Germany, **2** Institute of Animal Welfare, Ethology and Animal Hygiene, Faculty of Veterinary Medicine, Ludwig-Maximilians-University, Munich, Germany, **3** Laboratory of Retinal Cell Biology, University of Zurich, Zurich, Switzerland, **4** Neuromedical Genetics, Netherlands Institute for Neuroscience, Amsterdam, The Netherlands, **5** Toronto Western Research Institute, University Health Network, Departments of Ophthalmology and Visual Science, and Laboratory Medicine and Pathobiology, University of Toronto, Toronto, Ontario, Canada

Abstract

Background: Optical coherence tomography (OCT) is a novel method of retinal *in vivo* imaging. In this study, we assessed the potential of OCT to yield histology-analogue sections in mouse models of retinal degeneration.

Methodology/Principal Findings: We achieved to adapt a commercial 3rd generation OCT system to obtain and quantify high-resolution morphological sections of the mouse retina which so far required *in vitro* histology. OCT and histology were compared in models with developmental defects, light damage, and inherited retinal degenerations. In conditional knockout mice deficient in retinal retinoblastoma protein Rb, the gradient of *Cre* expression from center to periphery, leading to a gradual reduction of retinal thickness, was clearly visible and well topographically quantifiable. In *Nrl* knockout mice, the layer involvement in the formation of rosette-like structures was similarly clear as in histology. OCT examination of focal light damage, well demarcated by the autofluorescence pattern, revealed a practically complete loss of photoreceptors with preservation of inner retinal layers, but also more subtle changes like edema formation. In *Crb1* knockout mice (a model for Leber's congenital amaurosis), retinal vessels slipping through the outer nuclear layer towards the retinal pigment epithelium (RPE) due to the lack of adhesion in the subapical region of the photoreceptor inner segments could be well identified.

Conclusions/Significance: We found that with the OCT we were able to detect and analyze a wide range of mouse retinal pathology, and the results compared well to histological sections. In addition, the technique allows to follow individual animals over time, thereby reducing the numbers of study animals needed, and to assess dynamic processes like edema formation. The results clearly indicate that OCT has the potential to revolutionize the future design of respective short- and long-term studies, as well as the preclinical assessment of therapeutic strategies.

Citation: Fischer MD, Huber G, Beck SC, Tanimoto N, Muehlfriedel R, et al. (2009) Noninvasive, *In Vivo* Assessment of Mouse Retinal Structure Using Optical Coherence Tomography. PLoS ONE 4(10): e7507. doi:10.1371/journal.pone.0007507

Editor: Huibert D. Mansvelder, Vrije Universiteit Amsterdam, Netherlands

Received May 31, 2009; **Accepted** September 21, 2009; **Published** October 19, 2009

Funding: This work was supported by the Deutsche Forschungsgemeinschaft (DFG, grants Se837/5-2, Se837/6-1, Se837/7-1), the German Ministry of Education and Research (BMBF grant 0314106), the European Union grants LSHG-CT-512036 and EU HEALTH-F2-2008-200234, and a contribution of the Tistou and Charlotte Kerstan Foundation to the OCT equipment. The funders had no role in study design, data collection and analysis, decision to publish, or preparation of the manuscript.

Competing Interests: The authors have declared that no competing interests exist.

* E-mail: see@uni-tuebingen.de

¤a Current address: Novartis Pharma Schweiz AG, Berne, Switzerland
¤b Current address: VU University Medical Center, Department of Molecular Cell Biology and Immunology, Amsterdam, The Netherlands

☯ These authors contributed equally to this work.

Introduction

Mice are important model organisms in many areas of science. The retina as part of the brain offers the unique opportunity to directly visualize changes associated with neurodegenerative disorders and vascular alterations [1], or during the preclinical assessment of pharmacological approaches [2]. However, the current need to sacrifice animals for histological examinations at different time points interferes with the ability to follow the disease process and to monitor therapeutic or side effects over time in the same individuals.

Optical coherence tomography (OCT) is a novel method of retinal imaging [3]. Technically, OCT uses a weakly coherent infrared laser to analyze the reflectance properties of a sample [3]. The spectral domain mode (Fig. 1 A) currently outmatches the time domain mode as it combines high resolution with high recording speed. Each resulting data set consists of a large number of topographically ordered depth profiles (A-Scans), which together represent a two-dimensional slice (similar to an ultrasound scan) across the sample. Several consecutive slices together may be used to generate a three-dimensional data set ("volume scan").

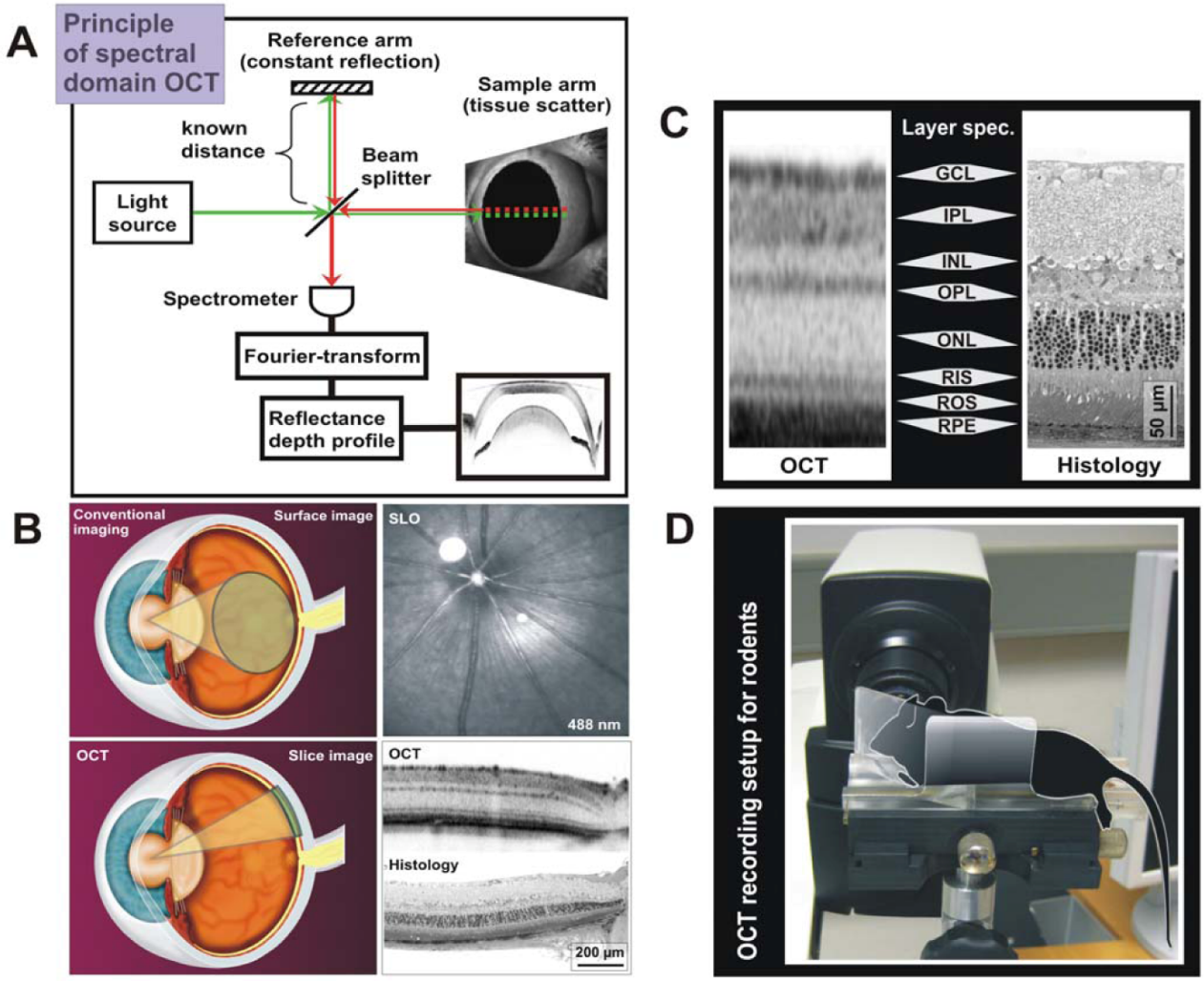

Figure 1. Principle of Optical Coherence Tomography (OCT) and its application in rodents. A) Schematic diagram of spectral-domain (SD) OCT. Green arrows indicate efferent, red arrows afferent light. **B)** Comparison of OCT to conventional ophthalmic imaging techniques. Top left: Conventional techniques either yield surface images of the retina (''fundus''), or in case of Scanning-Laser Ophthalmoscopy (SLO), confocal horizontal sections. Top right: Example of an SLO image of the central murine retina. Bottom left: In contrast, the OCT provides high-resolution vertical sections. Bottom right: Example of an OCT slice from the central murine retina in comparison to matching standard light microscopy. **C)** Representation of retinal layers in OCT and histology. See text for details. **D)** OCT recording setup for rodents. The schematic drawing of a mouse marks the recording position on the XYZ table. The eye is directly facing the OCT recording unit with a 78 dpt. lens attached.
doi:10.1371/journal.pone.0007507.g001

State-of-the-art imaging in rodents based on conventional fundus cameras or even confocal scanning-laser ophthalmoscopy (SLO) provides predominantly surface information but has a very restricted depth resolution [1] (Fig. 1B). This has been a severe limitation in animal studies. The OCT, in contrast, provides a high-resolution depth profile based on reflectivity that correlates well with histomorphological sections (Fig. 1C). However, the resulting image is different as conventional imaging and histology are based on absorption (light shade - little absorption, dark shade - strong absorption), whereas OCT is based on reflectivity (light shade - weak reflectivity, dark shade - strong reflectivity). In particular, membranous surfaces are extremely well detected in OCT regardless of their physical extension. Consequently, membrane-rich but less optically dense layers like plexiform and nerve-fiber layers are represented in a darker shade of gray than optically more dense layers with less membrane content like the outer nuclear layer (Fig. 1C). It is thus that the OCT provides not only refined depth resolution but also entirely new information about the sample structure.

Recent studies with custom-made equipment support the applicability of OCT in rodents, the ability to detect retinal lesions, and the potential to follow disease processes over time [4,5]. In this work, we adapted a high-resolution 3rd generation OCT system (Heidelberg Engineering Spectralis^{TM}) for use in small animal models to obtain detailed histology-analogue sections of the retina *in vivo*, without the need for an internal modification of the OCT device. This approach is superior to the use of custom-made experimental setups in terms of availability, reproducibility, familiarization, and standardization, and will thus be valuable for the future spread of this technique among the scientific community. The setup with an animal in place is shown in Fig. 1D and further described in the methods section.

Results

Following an initial comparison between OCT and histology in C57/BL6 wild-type mice, we have studied the representation of the phenotype in models with developmental defects (*Rb* gene), light damage, and inherited retinal degenerations (*Nrl* & *Crb1*genes).

Comparison of OCT and histology

The correspondence of layers in morphological OCT and histological sections (qualitatively shown in Fig. 1 D), was examined quantitatively in C57/BL6 wild-type mice (Fig. 2). No significant difference in layer thickness was detected between the two methods (Student's t-test at a significance level of $p<0.05$), and the best linear fit of the data yielded a correlation coefficient R^2 of 0.89 (Fig. 2 A). Due to differences in tissue processing techniques, the slope of the fit may vary between labs; it is thus important to obtain a set of local control data for own studies. The average dimensions of the individual layers are given in Fig. 2B, together with their respective standard deviations, further confirming the close agreement between histology and OCT.

Light damage

Photoreceptor apoptosis is a common final path of many inherited and induced retinal neurodegenerations. Typically, the outer retina mainly formed by photoreceptor cell bodies and their inner and outer segments degenerates and subsequently vanishes without major alterations of the inner retinal layers. Whereas inherited diseases commonly affect the retina gradually, i.e. the course of a degeneration takes some time and its topographical distribution may not be uniform, focal light exposure (particularly high intensity blue light) produces strictly localized lesions adjacent to practically normal retina within a short period of time [6], allowing a direct comparison between damaged and non-damaged areas (Figure 3 A). The huge amount of autofluorescent, lipid-rich debris from photoreceptor outer segments that cannot be processed by the retinal pigment epithelium and glial cells clearly demarcates the area of damage in SLO autofluorescence imaging (Fig. 3 B). The selective loss of the outer retina in the exposed region (marked with an asterisk) is very prominent (Fig. 3 C). Also, the transition zone (Fig. 3 D,E) closely matches that in a respective histomorphological section, but preserves the capability to follow the development of such degenerative changes over time, an important added value of *in vivo* diagnostics. A novel finding in rodents was the discovery of a site of edema formation (arrowhead in Fig. 3 E), a pathological alteration that does not endure the tissue processing required for *in vitro* methods, and is thus not visible in traditional histology. Edema was present in all (4/4) of the treated cases 3 days following the exposure, and was still present one week later (4/4). In all cases, it formed a ring around the light damage area. Edema is a common finding in human retinal diseases. Its appearance in OCT has been extensively studied, and these findings closely resemble the situation in our data [7].

Nrl knockout mouse

In the *Nrl* knockout mouse, the neural retina leucine zipper (*Nrl*) gene is impaired [8]. A major function of Nrl is to determine the fate of rod photoreceptor precursor cells, so that a lack of Nrl during development leads to an abnormal differentiation of these rod precursors into cone-like photoreceptors. The corresponding human disease, enhanced S-cone syndrome (ESCS), may either be caused by a lack of NRL or NR2E3, a transcription factor with overlapping functions to NRL [9]. A landmark of such retinas is

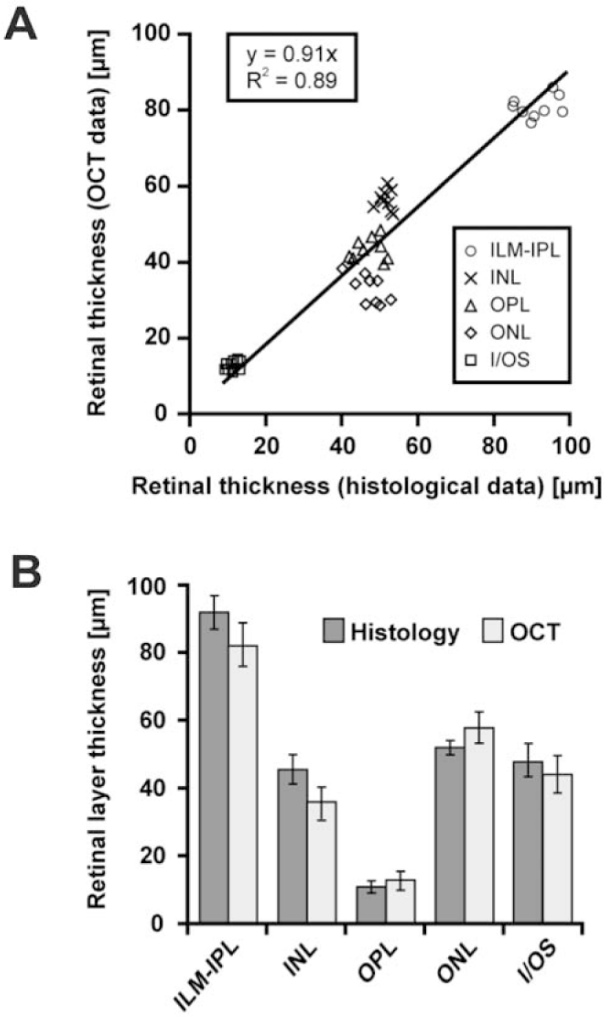

Figure 2. OCT and histological morphometric data in rodents. Relationship between OCT and histological morphometry in C57/BL6 mice broken down to retinal layers. **A)** Correlation of histological and OCT data. Pearson's correlation coefficient (R^2) is based on the data of all quantified retinal layers. **B)** Comparison of retinal layer thickness between histology (dark) and OCT (light). There was no statistically significant difference between histological analysis and OCT-based quantification in any retinal layer using Student's t-test at a significance level of $p<0.05$. All data are reported as mean values±standard deviation (error bars).
doi:10.1371/journal.pone.0007507.g002

the formation of rosettes [9,10], whose distribution can be assessed with conventional *in vivo* imaging as they present as whitish dots in native SLO (Fig. 4 A) and in autofluorescence mode (Fig. 4 B). The structure of the respective lesions becomes accessible with OCT both in humans [9] and mice (Fig. 4 C). As before, histomorphological and OCT data correlate well (Fig. 4 D). The detailed comparison (Fig. 4 E vs. Fig. 4 F) illustrates the difference in image appearance between reflection- and absorption-based methods discussed before (Fig. 1).

Crb1 knockout mouse

It is almost impossible to detect scattered lesions functionally, particularly in cases of vascular abnormalities without generalized hypoxia. In mutants lacking the Crumbs1 gene, the separation

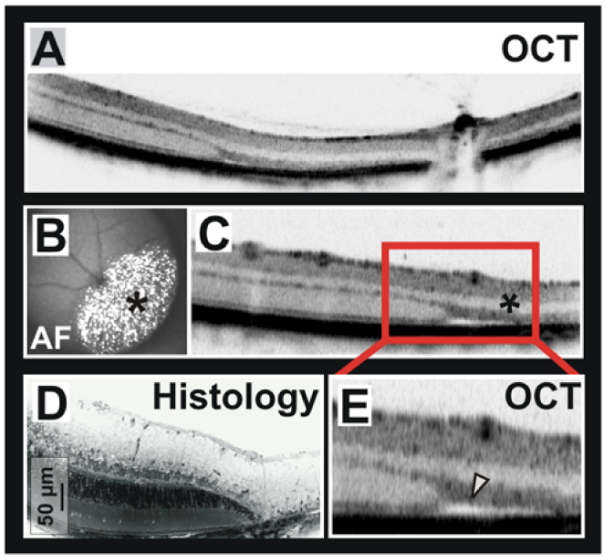

Figure 3. OCT assessment of light-induced murine retinal degeneration. A) OCT section across the central retina, containing adjacent damaged and non-damaged areas. **B)** Demarcation of the damaged area *in vivo* by SLO autofluorescence (AF) imaging based on fluorescent photoreceptor debris (marked by an asterisk). **C)** Detail of the transition zone between damaged and non-damaged retina in a). The asterisk marks the damaged area as in B). **D), E)** Comparison of the representation of light-induced retinal damage in histology and OCT. The arrowhead in the OCT image points towards a site of retinal edema.
doi:10.1371/journal.pone.0007507.g003

between inner and outer retina is weakened [11], allowing unnatural migration of cells and cell groups across gaps within that border [12]. It is believed that if a capillary vessel runs close to such a site, it may also descend into the vessel-free photoreceptor layer and eventually make contact with the retinal pigment epithelium (RPE). As the RPE produces VEGF, such aberrant vessels usually proliferate and appear in some cases to form connections with the choroidal vascular system. The sheer presence of such neovascularizations may be detected with traditional fluorescein angiography (FLA, Fig. 5 A, B). However, an accurate topographic reconstruction that allows to uncover the exact depth localization and the extent of the lesion is now feasible with the OCT (Fig. 5 C). This particular example further illustrates the capability to detect intraretinal (black arrows) as well as choroidal vessels (white arrows), which so far required a full histological work-up of such lesion sites (Fig. 3D).

Rb retina-specific knockout

Interference with the molecular patterning events during retinal development often results in cell-type specific dysmorphogenic alterations. An example is the retinoblastoma protein (Rb), an important tumor suppressor, that blocks cell division and death by inhibiting the E2f transcription factor family, leading to apoptosis of a large fraction of retinal cells [13]. As factors like Rb often have related functions in many different tissues, a complete loss of respective genes commonly leads to embryonic lethality, preventing the generation of knock-out models. However, organ-specific models are often possible to obtain on the basis of the Cre-*lox* P system, where the gene to be deleted is solely removed in tissues that express Cre recombinase [14]. In this work, we used $Rb^{loxP/loxP}$; α-*Cre* mice where the floxed *Rb* exon 19 is only deleted in the retina at embryonic day E10 [15]. However, the expression of the α-*Cre*

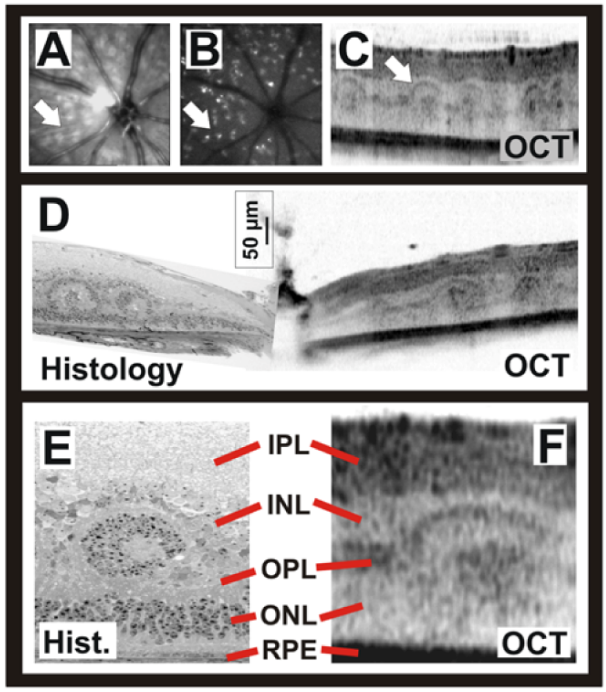

Figure 4. Capability of the OCT to detect and capture the nature of lesions. A)–F) Multiple retinal rosette formation in the neural retinal leucine zipper (*Nrl*) knockout mouse. **A)** SLO surface image (514 nm) in which the retinal rosettes (arrow) show as whitish dots. **B)** SLO autofluorescence image indicating that the rosettes contain fluorescent material. **C)** Representative OCT slice of a *Nrl* knockout mouse revealing details of the nature of the rosettes (arrow) and their depth localization. **D)** Comparison of the OCT representation of *Nrl* rosettes with histology (different individual animal). **E, F)** Detail illustrating how well retinal structures in OCT and histology correlate.
doi:10.1371/journal.pone.0007507.g004

transgene is not topographically homogeneous in this mouse model [16], leading to different degrees of gene inactivation within the same organ. In particular, the retinal periphery shows the full effect of Rb loss, whereas there is almost no α-*Cre* transgene activity in the central retina. Here, we took advantage of this Cre recombinase distribution pattern to ascertain the transition effect between the central area with regular development and more peripheral parts with developmental apoptosis within the same retinal slice (Fig. 6). Despite the somewhat lower resolution achievable in living tissues, the changes in retinal layering and thickness associated with *Rb* gene loss appeared equally well ascertainable with histology and OCT (Figure 6 A vs. B). An important feature of OCT is the capability to capture multiple (Fig. 6 C) sections directly linked to the surface image within a short period of time, allowing to follow topographical changes like the thickness gradient from center to periphery. A set of consecutive serial sections ("volume scan") even allows this gradient to be mapped (Fig. 6 D), which in this case correlates with the topography of α-*Cre* transgene expression *in vivo*.

Discussion

In this work, we assessed the scientific benefit of the OCT in rodent models featuring retinal neurodegeneration, perturbed retinal structure, neovascular conditions, and developmental aberrations, all likely fields of interest to a wide range of academic and industrial researchers.

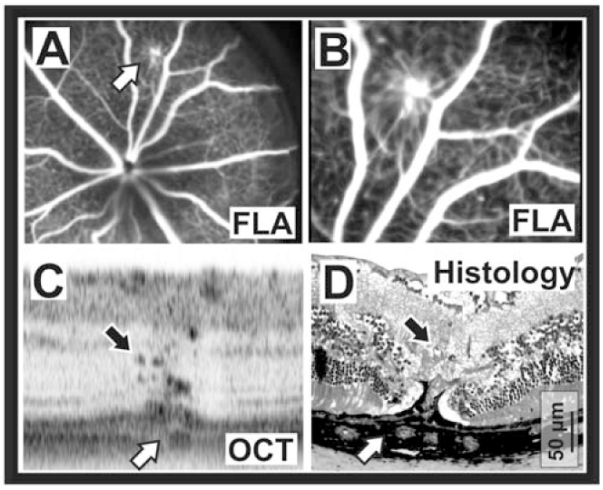

Figure 5. Capability of the OCT to detect and capture the nature of lesions. A)–D) Site of neovascularization in a Crumbs 1 (*Crb1*) knockout mouse. **A)** SLO fluorescence angiographic (FLA) image of a retinal neovascular site (arrow) in a representative *Crb1* knockout mouse. **B)** Detail of g) illustrating the traction the aberrant vessel applies to the neighboring capillaries. **C)** Representative OCT slice depicting enlarged aberrant retinal vessels (black arrow) as well as choroidal vascular changes (white arrow) at the same position, implicating a connection between both vascular beds. **D)** Histological section of the above neovascular site for comparison. The black arrow points to aberrant retinal vessels, and the white arrow to choroidal changes.
doi:10.1371/journal.pone.0007507.g005

The results in the light damaged retina show the benefit of the combination of surface imaging with the SLO for aiming at sites of interest (like here demarcated by autofluorescence) and the OCT. We found a close correlation of the site of autofluorescence in the 488 nm SLO images (attributed to the lipid-rich remnants of the photoreceptor outer segments) with the outer retinal damage in the OCT sections. For the first time, we were able to demonstrate edema formation in these rodents (Fig. 3 E), which appears to be part of the dynamic processes associated with acute light exposure and, because of the tissue processing, is not detectable in conventional morphological analyses.

An example of perturbed retinal structure is the rosette formation in the *Nrl* knockout mouse (Fig. 4). Whereas the relatively even topographical distribution of the lesions became visible in SLO imaging (similar to a retinal whole-mount, Fig. 4 A,B), details of the structure were accessible *in vivo* with OCT sections (Fig. 4 E,F). The formation of rosettes in Nrl mutants is not yet fully understood, but it is known that cones are a major component of these dysmorphic structures, with their inner and outer segments pointing towards the center of each rosette [10]. The respective photoreceptor nuclei around the center of the rosette in Fig. 4E (similar to the ONL ones) correspond in the OCT to an area of low reflectivity in Fig. 4F (similar to the ONL band). The center of rosettes was further shown to contain RPE proteins and have connections to the RPE layer [10]. In the OCT, we found that this tissue has reflective properties close to plexiform layers (Fig. 4F). Rosette formation occurs postnatally [10,17], apparently driven by a metabolic need of the retina, leading to an increased surface area between RPE and photoreceptors. To better understand this process, we will examine the time course in individual animals in a separate study.

In mutants lacking the *Crumbs1* gene, lesions are commonly sparse (Fig. 5 A), which makes an histological analysis laborious and demanding. An *in vivo* screening with the SLO has proven to be very effective the overall assessment as well as a preselection for immunostainings, saving time, money, and animals. Now, with the OCT, the nature and extent of the lesions can be assessed in real time. The particular example in Fig 5 C illustrates the capability to detect intraretinal (black arrows) as well as choroidal vessels (white arrows), which so far required a full histological work-up of such lesion sites (Fig. 5 D). Having the morphological information

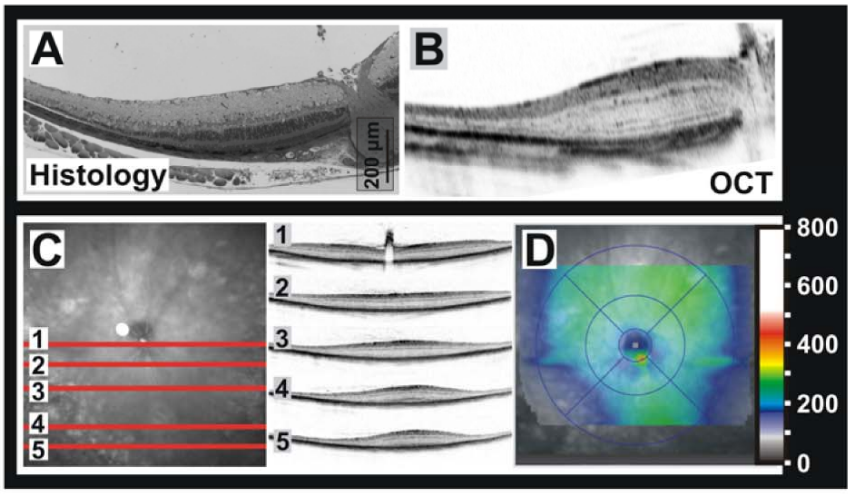

Figure 6. Topographic analysis of retinal thickness in an organ-specific model of retinoblastoma protein (*Rb*) deficiency. Thickness variations (center vs. periphery) were caused by imperfections of the Cre-lox system (see text), leading to differences in developmental apoptosis. **A)** Histological section across the central retina showing the smooth transition between centrally normal and peripherally reduced thickness. **B)** OCT section of the same region, the retinal thickness correlating well with the histomorphological data. **C)** Assessment of the gradual changes of retinal thickness from center to (mid)periphery based on 5 manually placed OCT slices. Left: SLO image of the fundus region with the position of the slices superimposed. Right: OCT slices at the positions indicated, ordered from center to periphery. **D)** Topography of retinal thickness calculated from 92 equidistant OCT slices ("volume scan" data). The color scale values are in µm.
doi:10.1371/journal.pone.0007507.g006

available *in vivo* permits to study the dynamics of such sites in more detail (together with the use of dyes) before the animal is sacrificed.

The results in the $Rb^{loxP/loxP}$;*α-Cre* mice illustrate how the developmental apoptosis due to an imbalance of RB and the E2Fs [13,15] affects the different layers (Fig. 6).

However, developmental apoptosis only occurs in areas where *Rb* is missing, which in this conditional knock-out is the area of Cre expression [14]. Since the retina-specific α-*Cre* mice used here do show a central-peripheral expression gradient, so does the apoptosis and, subsequently, retinal thickness. So, besides the *Rb*-specific findings, this model also helped to assess the feasibility of a topographical mapping of retinal thickness based on a set of consecutive serial sections (''volume scan''). The color-coded map (Fig. 6 D) reveals regular retinal thickness values mainly around the optic disc (image center), which reflects the inverse topography of the α-*Cre* transgene expression [16]. Thickness maps are further useful to follow thickness changes over time.

The prime advantage of OCT is certainly the ability to non-invasively produce histology-analogue retinal sections. As we have shown, these are both useful for the assessment and numerical quantification of generalized changes and for the detection and analysis of sporadic, localized lesions.

In many cases, standard histology may be replaced or at least its extent reduced by OCT, diminishing the amount of study animals needed. Even if histological sections are required (e.g. immuno-stains), OCT may help to preselect and to determine the optimal time point in individual animals in case of progressive changes.

As most degenerative processes are dynamic in nature, the non-invasive examination has substantial advantages for the understanding of short–term alterations like edema formation. A requirement for preclinical and long-term studies is that markers of potential degenerative changes or therapeutic effects may be analyzed numerically. The OCT, for the first time, allows an accurate quantitative description of the retinal layers *in vivo* as shown in Fig. 2. As the majority of lesions primarily compromise the outer retina but leave the inner retina unchanged, it is a fundamental improvement that these layers are now accessible to separate quantification.

In summary, our results present the OCT as an important new tool for the *in vivo* analysis of rodent eyes. It is not only a methodological step forward but will also significantly help to reduce standard histology and thus the amount of animals needed. The ability to monitor developmental as well as inherited and induced degenerative processes and respective therapeutic intervention in the same individual animals opens a wide field of applicability in future long-term and preclinical studies. In conjunction with other non-invasive tests like electroretinography (ERG), OCT allows for a refined morphological and functional follow-up over time.

Methods

Animals

All procedures concerning animals adhered to the ARVO statement for the use of animals in ophthalmic and vision research, and were performed with permission of local authorities (Regierungspraesidium Tuebingen). All mice were kept under a 12 h:12 h light-dark cycle (60 lux), had free access to food and water and were used irrespective of gender.

Optical adaptation to the mouse eye

Retinal imaging of the mouse eye with its small pupil has been a challenge because of the difficult alignment of light delivered to the eye. The small aperture also reduces the amount of light which is reflected from the retina, and therefore decreases the signal-to-noise ratio [18]. Over a decade of SLO in vivo imaging in animals, we have tested several conditions for the visualization of the murine fundus. We found that a basic setup containing only two additional lenses is sufficient to obtain very good quality results without the need to modify the equipment internally (Figure 1D). All SLO and OCT images in this work were recorded using this setup. On the SLO/OCT side, a 78 diopter double aspheric lens (Volk Optical, Inc., Mentor, OH 44060, U.S.A.) is fixed directly to the outlet of the device. To the eye of the mouse, a custom-made contact lens with a focal length of 10 mm is applied with a drop of methyl cellulose (Methocel 2%, OmniVision, Puchheim, Germany). Mouse eye and equipment must be aligned correctly, e.g. by means of a XYZ table, and brought closely together, so that they almost touch.

Scanning-laser ophthalmoscopy and angiography

For en face retinal imaging, we used the commercially available HRA 1 and HRA 2 systems (Heidelberg Engineering, Dossenheim, Germany) featuring up to two Argon wavelengths (488 and 514 nm) in the short wavelength range and two infrared diode lasers (HRA 1: 795 and 830 nm, HRA 2: 785 and 815 nm) in the long wavelength range. The 488 and 795 nm lasers are used for fluorescein (FLA) and indocyanine green (ICG) angiography, respectively. Appropriate barrier filters at 500 and 800 nm remove the reflected light with unchanged wavelength while allowing only the light emitted by the dye upon stimulation to pass through.[1]

A detailed protocol for anesthesia and conventional imaging is described elsewhere [1]. Briefly, mice were anaesthetized by subcutaneous injection of ketamine (66.7 mg/kg) and xylazine (11.7 mg/kg) and their pupils dilated with tropicamide eye drops (Mydriaticum Stulln, Pharma Stulln, Stulln, Germany) before image acquisition.

Spectral domain Optical Coherence Tomography

SD-OCT imaging was done in the same session as cSLO to minimize variability. For OCT imaging, we used a commercially available Spectralis^{TM} HRA+OCT device from Heidelberg Engineering featuring a broadband superluminescent diode at $\lambda = 870$ nm as low coherent light source.

Each two-dimensional B-Scan, recorded with the equipment set to 30° field of view, consists of 1536×496 pixels, which are acquired at a speed of 40,000 scans per second. Optical depth resolution is ca. 7 μm with digital resolution reaching 3.5 μm [19]. The combination of scanning laser retinal imaging and SD-OCT allows for real-time tracking of eye movements and real-time averaging of OCT scans, reducing speckle noise in the OCT images considerably. Resulting data were exported as 24 bit color bitmap files and processed in Adobe Photoshop CS2 (Adobe Systems, San Jose, CA, U.S.A.).

Analysis of retinal morphology

Animals were sacrificed and enucleated for histological analysis. After orientation was marked, the eyes were fixed overnight in 2.5% gluteraldehyde prepared in 0.1 M cacodylate buffer and processed as prescribed previously [20]. Semi-thin sections (0.5 mm) of Epon-embedded tissue were prepared form the central retina, counterstained with methylene blue and analyzed using a light microscope (Axiovision, Zeiss, Jena, Germany).

Author Contributions

Conceived and designed the experiments: MDF MWS. Performed the experiments: MDF GH SB NT RM EF CG AW CER SAvdP JW MWS.

Analyzed the data: MDF GH SB NT RM EF CG AW CER SAvdP JW MP RB MWS. Contributed reagents/materials/analysis tools: MDF GH SB NT RM EF CG AW CER SAvdP JW MP RB MWS. Wrote the paper: MWS. Edited the manuscript: CG AW CER SAvdP JW MP RB.

References

1. Seeliger MW, Beck SC, Pereyra-Muñoz N, Dangel S, Tsai JY, et al. (2005) *In vivo* confocal imaging of the retina in animal models using scanning laser ophthalmoscopy. Vision Res 45: 3512–3519.
2. Edelhauser HF, Boatright JH, Nickerson JM, Third ARVO/Pfizer Research Institute Working Group (2008) Drug delivery to posterior intraocular tissues: third Annual ARVO/Pfizer Ophthalmics Research Institute Conference. Invest Ophthalmol Vis Sci 49: 4712–4720.
3. Fujimoto JG (2003) Optical coherence tomography for ultrahigh resolution *in vivo* imaging. Nat Biotechnol 21: 1361–1367.
4. Kim KH, Puoris'haag M, Maguluri GN, Umino Y, Cusato K, et al. (2008) Monitoring mouse retinal degeneration with high-resolution spectral-domain optical coherence tomography. J Vis 24: 17,1–11.
5. Xu J, Molday LL, Molday RS, Sarunic MV (2009) In vivo imaging of the mouse model of X-linked juvenile retinoschisis with fourier domain optical coherence tomography. Invest Ophthalmol Vis Sci 50: 2989–2993.
6. Wenzel A, Grimm C, Samardzija M, Remé CE (2005) Molecular mechanisms of light-induced photoreceptor apoptosis and neuroprotection for retinal degeneration. Prog Retin Eye Res 24: 275–306.
7. Barthelmes D, Sutter FK, Gillies MC (2008) Differential optical densities of intraretinal spaces. Invest Ophthalmol Vis Sci 49: 3529–3534.
8. Mears AJ, Kondo M, Swain PK, Takada Y, Bush RA, et al. (2001) Nrl is required for rod photoreceptor development. Nat Genet 29: 447–452.
9. Wang NK, Fine HF, Chang S, Chou CL, Cella W, et al. (2009) Cellular origin of fundus autofluorescence in patients and mice with a defective NR2E3 gene. Br J Ophthalmol 93: 1234–1240.
10. Wenzel A, von Lintig J, Oberhauser V, Tanimoto N, Grimm C, et al. (2007) RPE65 is essential for the function of cone photoreceptors in NRL-deficient mice. Invest Ophthalmol Vis Sci 48: 534–542.
11. van de Pavert SA, Kantardzhieva A, Malysheva A, Meuleman J, Versteeg I, et al. (2004) Crumbs homologue 1 is required for maintenance of photoreceptor cell polarization and adhesion during light exposure. J Cell Sci 117: 4169–4177.
12. van de Pavert SA, Sanz AS, Aartsen WM, Vos RM, Versteeg I, et al. (2007) Crb1 is a determinant of retinal apical Müller glia cell features. Glia 55: 1486–1497.
13. Chen D, Livne-bar I, Vanderluit JL, Slack RS, Agochiya M, et al. (2004) Cell-specific effects of RB or RB/p107 loss on retinal development implicate an intrinsically death-resistant cell-of-origin in retinoblastoma. Cancer Cell 5: 539–551.
14. Sauer B (1998) Inducible gene targeting in mice using the Cre/lox system. Methods 14: 381–392.
15. Chen D, Opavsky R, Pacal M, Tanimoto N, Wenzel P, et al. (2007) Rb-Mediated Neuronal Differentiation through Cell-Cycle-Independent Regulation of E2f3a. PLoS Biol 5: e179.
16. Bäumer N, Marquardt T, Stoykova A, Ashery-Padan R, Chowdhury K, et al. (2002) Pax6 is required for establishing naso-temporal and dorsal characteristics of the optic vesicle. Development 129: 4535–4545.
17. Feathers KL, Lyubarsky AL, Khan NW, Teofilo K, Swaroop A, et al. (2008) Nrl-knockout mice deficient in Rpe65 fail to synthesize 11-cis retinal and cone outer segments. Invest Ophthalmol Vis Sci 49: 1126–1135.
18. Ruggeri M, Wehbe H, Jiao S, Gregori G, Jockovich ME, et al. (2007) Invest Ophthalmol Visual Sci 48: 1808–1814.
19. Wolf-Schnurrbusch UE, Enzmann V, Brinkmann CK, Wolf S (2008) Invest Ophthalmol Vis Sci 49: 3095–3099.
20. Samardzija M, Wenzel A, Aufenberg S, Thiersch M, Reme C, et al. (2006) FASEB J 20: 2411–2413.

IV. MANUSCRIPT

Investigative Ophthalmology and Visual Science

First published on Aug 6th, 2009 as doi:10.1167/iovs.09-3724

Spectral Domain Optical Coherence Tomography in Mouse Models of Retinal Degeneration

Gesine Huber, Susanne Christine Beck, Christian Grimm, Ayse Sahaboglu-Tekgoz, Francois Paquet-Durand, Andreas Wenzel, Peter Humphries, T. Michael Redmond, Mathias W. Seeliger, and M. Dominik Fischer

Spectral Domain Optical Coherence Tomography in Mouse Models of Retinal Degeneration

Gesine Huber,[1,2] *Susanne C. Beck,*[1] *Christian Grimm,*[3] *Ayse Sahaboglu-Tekgoz,*[4] *Francois Paquet-Durand,*[4] *Andreas Wenzel,*[3,5] *Peter Humphries,*[6] *T. Michael Redmond,*[7] *Mathias W. Seeliger,*[1,8] *and M. Dominik Fischer*[1,8]

Purpose. Spectral domain optical coherence tomography (SD-OCT) allows cross-sectional visualization of retinal structures in vivo. Here, the authors report the efficacy of a commercially available SD-OCT device to study mouse models of retinal degeneration.

Methods. C57BL/6 and BALB/c wild-type mice and three different mouse models of hereditary retinal degeneration (*Rho*$^{-/-}$, *rd1*, *RPE65*$^{-/-}$) were investigated using confocal scanning laser ophthalmoscopy (cSLO) for en face visualization and SD-OCT for cross-sectional imaging of retinal structures. Histology was performed to correlate structural findings in SD-OCT with light microscopic data.

Results. In C57BL/6 and BALB/c mice, cSLO and SD-OCT imaging provided structural details of frequently used control animals (central retinal thickness, $CRT_{C57BL/6} = 237 \pm 2$ μm and $CRT_{BALB/c} = 211 \pm 10$ μm). *RPE65*$^{-/-}$ mice at 11 months of age showed a significant reduction of retinal thickness ($CRT_{RPE65} = 193 \pm 2$ μm) with thinning of the outer nuclear layer. *Rho*$^{-/-}$ mice at P28 demonstrated degenerative changes mainly in the outer retinal layers ($CRT_{Rho} = 193 \pm 2$ μm). Examining *rd1* animals before and after the onset of retinal degeneration allowed monitoring of disease progression ($CRT_{rd1\ P11} = 246 \pm 4$ μm, $CRT_{rd1\ P28} = 143 \pm 4$ μm). Correlation of CRT assessed by histology and SD-OCT was high ($r^2 = 0.897$).

Conclusions. The authors demonstrated cross-sectional visualization of retinal structures in wild-type mice and mouse models for retinal degeneration in vivo using a commercially available SD-OCT device. This method will help to reduce numbers of animals needed per study by allowing longitudinal study designs and will facilitate characterization of disease dynamics and evaluation of putative therapeutic effects after experimental interventions. (*Invest Ophthalmol Vis Sci.* 2009;50: 000–000) DOI:10.1167/iovs.09-3724

Optical coherence tomography (OCT) has evolved over the past two decades to become an important diagnostic tool in clinical ophthalmology and other medical specialties.[1] Widespread application of this powerful tool in animal research, however, was restricted because of poor image quality in commercially available first- and second-generation time domain OCT devices.[2,3] Sufficiently high image quality could be achieved only with prototype devices with improved depth resolution that were specifically adapted for the respective animal visual system.[4–7] Only recently, latest generation SD-OCT devices have become commercially available that provide scanning speed and depth resolution sufficient for small animal experimentation.[8] Given that SD-OCT is ideally suited for studying changes of retinal integrity, wild-type mice and mouse models of retinal degeneration were chosen to explore the efficacy of this method.

Thus far, animal models of retinal degeneration have been studied extensively on both functional and structural levels. Morphologic changes were detected using either en face imaging methods such as funduscopy[9] and confocal scanning laser ophthalmoscopy (cSLO)[10] or, more commonly, ex vivo histologic approaches. Although light and electron microscopy provide (ultra-)high structural resolution, fixation procedures, dehydration preparatory to subsequent embedding, and staining, even the processes of cutting, flattening, and mounting histologic sections are potential sources for significant and variable alterations in dimensions.[11,12] Indeed, retinal thickness measures of rodent retina are reported to be 95 μm in one study[13] and 170 to 217 μm in other studies.[11,14] Taken together, ex vivo analysis of retinal tissue has certain limitations and should be interpreted accordingly. In vivo analysis of the retina has significant benefits as delicate, but functionally important changes such as retinal edema and focal neurosensory and pigment epithelial detachments can readily be detected by SD-OCT while potentially remaining undetected or masked by handling procedures in histologic analysis. Finally, monitoring of dynamic changes in individual animals requires a noninvasive study design. Here, SD-OCT has the potential to complement the existing in vivo methods in vision research by providing histology-analog structural details on retinal integrity. Because individual animals may be investigated at multiple time points, SD-OCT can also help to reduce the numbers of animals needed for such a study, which has both ethical and economic implications. To the best of our knowledge, this is the first study to demonstrate the efficacy of a commercially

From the [1]Division of Ocular Neurodegeneration and the [4]Division for Experimental Ophthalmology, Institute for Ophthalmic Research, Centre for Ophthalmology, Tuebingen, Germany; [2]Institute of Animal Welfare, Ethology and Animal Hygiene, Faculty of Veterinary Medicine, Ludwig-Maximilians-University, Munich, Germany; [3]Laboratory of Retinal Cell Biology, Department of Ophthalmology, University of Zurich, Zurich, Switzerland; [6]Ocular Genetics Unit, Trinity College, Dublin, Ireland; and [7]National Eye Institute, National Institutes of Health, Bethesda, Maryland.

[8]These authors contributed equally to the work presented here and should therefore be regarded as equivalent authors.

[5]Present affiliation: Novartis Pharma Schweiz AG, Bern, Switzerland.

Supported by Deutsche Forschungsgemeinschaft Grants Se837/5–2, Se837/6–1, Se837/7–1, and PA1751/1–1; German Ministry of Education and Research Grant 0314106; European Union Grants LSHG-CT-512036 and EU HEALTH-F2–2008-200234, Kerstan Foundation, EU (MEST-CT-2005–020235).

Submitted for publication March 17, 2009; revised May 29, 2009; accepted Month Day, 2009.

Disclosure: **G. Huber**, None; **S.C. Beck**, None; **C. Grimm**, None; **A. Sahaboglu-Tekgoz**, None; **F. Paquet-Durand**, None; **A. Wenzel**, Novartis Pharma Schweiz (E); **P. Humphries**, None; **T.M. Redmond**, None; **M.W. Seeliger**, None; **M.D. Fischer**, None

The publication costs of this article were defrayed in part by page charge payment. This article must therefore be marked "*advertisement*" in accordance with 18 U.S.C. §1734 solely to indicate this fact.

Corresponding author: M. Dominik Fischer, Institute for Ophthalmic Research, Centre for Ophthalmology, University of Tuebingen, 72076 Tuebingen, Germany; dominik.fischer@med.uni-tuebingen.de.

available SD-OCT device to obtain cross-sectional images from wild-type mice and mouse models of retinal degeneration.

Materials and Methods

Animals

Animals were housed under standard white cyclic lighting (200 lux), had free access to food and water, and were used irrespective of gender. *Rho*$^{-/-}$[15] (n = 46), *RPE65*$^{-/-}$[16] (n = 10), BALB/c (n = 15; Charles River Laboratories), C57/BL6/J (n = 37; Charles River Laboratories), C3H *rd1/rd1* (n = 6, *rd1*), and control C3H wild-type (n = 6) mice[17] were used for imaging. All procedures were performed in accordance with the local ethics committee, German laws governing the use of experimental animals, and the ARVO Statement for the Use of Animals in Ophthalmic and Vision Research. Because of the critical changes after postnatal day (P) 11,[18,19] imaging in *rd1* and corresponding wild-type were carried out at P11 and P28. Because of the later onset and slower course of degeneration in the *Rho*$^{-/-}$ *and RPE65*$^{-/-}$ mouse models, imaging was performed at 1 and 11 months, respectively.

Confocal Scanning Laser Ophthalmoscopy

For en face retinal imaging, we used the commercially available HRA 1 and HRA 2 (Heidelberg Engineering, Heidelberg, Germany) featuring up to two argon wavelengths (488/514 nm) in the short-wavelength range and two infrared diode lasers (HRA 1, 795/830 nm; HRA 2, 785/815 nm) in the long-wavelength range. A detailed protocol for anesthesia and imaging is described elsewhere.[10] Briefly, mice were anesthetized by subcutaneous injection of ketamine (66.7 mg/kg) and xylazine (11.7 mg/kg), and their pupils were dilated with tropicamide eye drops (Mydriaticum Stulln; Pharma Stulln GmbH, Stulln, Germany) before image acquisition. By applying hydroxypropyl methylcellulose (Methocel 2%; OmniVision, Puchheim, Germany) on the eye, the refractive power of the air corneal interface was effectively negated. A custom-made contact lens (focal length, 10 mm) was used to reduce the risk of corneal dehydration and edema and to act as a collimator.

Spectral Domain Optical Coherence Tomography

SD-OCT imaging was performed in the same session as cSLO (i.e., animals remained anesthetized using identical preparatory steps). Mouse eyes were subjected to SD-OCT with a commercially available HRA+OCT device (Spectralis; Heidelberg Engineering, Heidelberg, Germany) featuring a broadband superluminescent diode at λ = 880 nm as a low coherent light source. Each two-dimensional B-scan recorded at 30° field-of-view consists of 1536 A-scans acquired at a speed of 40,000 scans per second. Optical depth resolution is approximately 7 μm, with digital resolution reaching 3.5 μm.[8]

To adapt for the optical qualities of the mouse eye, we mounted a commercially available 78-D double aspheric fundus lens (Volk Optical, Inc., Mentor, OH) directly in front of the camera unit. Imaging was performed with a proprietary software package (Eye Explorer, version 3.2.1.0; Heidelberg Engineering). Length of the reference pathway was adjusted manually according to manufacturer's instructions using the "OCT debug window" (press Ctrl/Shift/Alt/O simultaneously to open window in the active, calibrated OCT mode) to adjust for the optical length of the scanning pathway. The combination of scanning laser retinal imaging and SD-OCT allows for real-time tracking of eye movements and real-time averaging of OCT scans, reducing speckle noise in the OCT images considerably.[8] Resultant data were exported as 8-bit grayscale image files and were processed with a graphics editing program (Photoshop CS2; Adobe Systems, San Jose, CA). For quantification of central retinal thickness based on high-resolution volume scans, we used the proprietary software (Eye Explorer; Heidelberg Engineering). Briefly, each volume scan consisted of at least 70 B-scans recorded at 30° field-of-view centered on the optic disc, which were used to calculate an interpolated retinal thickness map across the scanned retinal area. Central retinal thickness was quantified using the circular OCT grid subfield at 3-mm diameter, with the center located on the optic disc.

Histology

Three animals from each mouse line (*Rho*$^{-/-}$, *RPE65*$^{-/-}$, BALB/c, and C57/BL6) were killed, and their eyes were enucleated for histologic analysis. After orientation was marked, the eyes were fixed overnight in 2.5% glutaraldehyde prepared in 0.1 M cacodylate buffer and were processed as described previously.[20] Semithin sections (0.5 mm) of Epon-embedded tissue were prepared form the central retina, counterstained with methylene blue, and analyzed using a light microscope (Axiovision; Zeiss, Jena, Germany).

For the timeline analysis of *rd1* mice (n = 3 for each group: rd1 P11, rd1 P28, wild-type P11, and wild-type P28), eyes were embedded unfixed in Jung tissue freezing medium (Leica Microsystems, Wetzlar, Germany), frozen, and sectioned (14 μm) in a cryotome (HM560; Microm, Walldorf, Germany). Sections were then stained using hematoxylin/eosin staining. Morphologic observations and light microscopy were performed on a microscope (Imager.Z1 Apotome; Zeiss) equipped with a digital camera (Axiocam MrN; Zeiss). Images were captured using corresponding software (Axiovision 4.6; Zeiss).

SD-OCT versus Histology

For correlation of retinal thickness measurements, *inner retina* was defined as ranging from the inner limiting membrane to the outer plexiform layer (OPL) and *outer retina* was defined as ranging from the outer nuclear layer (ONL) to the retinal pigment epithelium (RPE). In case of morphometric assessment of histologic sections, all measurements were taken at 1.4 mm eccentricity from the optic nerve head to mirror the SD-OCT-based thickness measurement along a circular ring scan (r = 1.4 mm) centered on the optic nerve head. Respective thickness was quantified by computer-assisted manual segmentation analysis using the proprietary software (Eye Explorer; Heidelberg Engineering) for SD-OCT data and the calibrated "line-tool" in Adobe (Photoshop CS2) for histologic micrographs.

Student's t-test was used to analyze statistical significance between respective inner and outer retinal thickness measurements (C57/Bl6 vs. *Rho*$^{-/-}$, *RPE65*$^{-/-}$, or BALB/c; C3H wild-type vs. C3H rd1/rd1 at P11 and P28). Correlation between thickness measurements by OCT versus histology was assessed by Pearson's correlation coefficient.

Results

C57BL/6

A basic examination using cSLO en face imaging was performed in 4-week-old C57BL/6 mice to confirm the presence of regular retinal and vascular structures typical for normal wild-type animals. The examination included native red-free (RF; 513 nm), infrared (IR; 830 nm), and autofluorescence (AF) modes fluorescein angiography and indocyanine green angiography (Fig. 1). The cross-sectional SD-OCT imaging in these animals provided detailed in vivo data on retinal layer composition (Fig. 1) and retinal thickness. In a central circular area of approximately 3-mm diameter, total retinal thickness was 237 $\pm$ 2 μm (mean $\pm$ SD). The laminar organization of the murine retina, as determined in vivo by SD-OCT, correlated well with ex vivo light microscopy studies (Fig. 1). Notably, some wild-type mice feature Bergmeister's papilla, a structural remnant of the developmental hyaloid vascular system (HVS) at the optic disc.[21] Indeed, angiography showed characteristic perfusion of the HVS in mice until approximately P10 (data not shown), after which the hyaloid artery usually obliterates and leaves behind the channel of Cloquet.[22] In some animals, however, this development remains incomplete, leading to Bergmeister's papilla, as seen in Figure 1F.

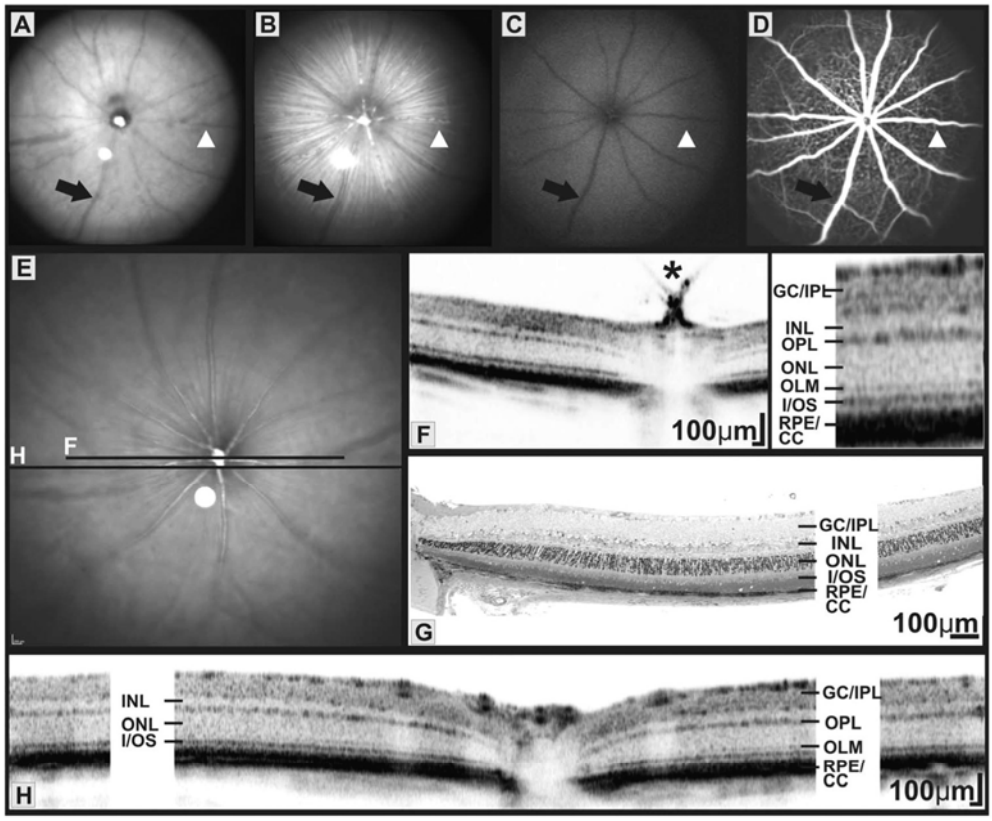

FIGURE 1. Retinal SLO imaging and OCT in C57BL/6 mice (PW4) with a regular retinal structure. (**A–D**) Representative example of en face imaging using cSLO. (**A**) Native IR (830 nm), (**B**) RF (513 nm), and (**C**) AF mode. (**D**) Fluorescein angiography (FLA) confirming an intact retinal vasculature (*arrowhead*, artery; *arrow*, vein). (**E–H**) Corresponding OCT data. (**E**) Fundus picture with indicated orientation of cross-sectional SD-OCT scans. (**F**) Corresponding B-scan at the optic nerve head displaying a Bergmeister's papilla characterized by a structural remnant of the developmental hyaloid vascular system (*asterisk*), including enlarged image. (**G**) Light microscopic data of an age-matched C57BL/6 animal. (**H**) Representative B-scan with retinal layers labeled. GC/IPL, ganglion cell/inner plexiform layer; OLM, outer limiting membrane; RPE/CC, RPE/choriocapillary complex.

BALB/c

En face imaging in BALB/c mice (postnatal week [PW]10) using cSLO showed nonpigmented retinal structures in the native RF (513 nm), IR (830 nm), and AF modes (Fig. 2). Given that BALB/c mice are highly susceptible to light-induced retinal degeneration,[23,24] the hyperfluorescent dots in the AF mode may reflect lipid degradation products. Accordingly, overall retinal thickness in the central 3 mm, as determined by SD-OCT, was 211 ± 10 µm, considerably less than in the C57BL/6 strain, which would be hypothetically consistent with a mild light-induced photoreceptor loss. Virtual cross-sections displayed identical laminar organization in the inner retina compared with C57BL/6. However, because lack of pigmentation in BALB/c mice resulted in altered optical characteristics in the outer retina, signal composition of SD-OCT scans distal of the external limiting membrane (ELM) differed considerably (Fig. 2). Specifically, instead of two highly reflective layers (HRLs) thought to represent the inner/outer segment border (I/OS) and RPE (Fig. 1), SD-OCT scans in BALB/c mice demonstrated two additional HRLs possibly demarcating the nonpigmented choriocapillary and choroidal structures (Fig. 2).

Rho$^{-/-}$

The visual pigment of the rod photoreceptors, rhodopsin, is an essential element of the phototransduction cascade and serves as a structural protein of the discs in the rod outer segments (ROS). Hence, in rhodopsin-deficient mice (*Rho*$^{-/-}$), ROS are never formed, and rod-derived ERG signals cannot be generated.[15] En face imaging in *Rho*$^{-/-}$ mice (PW4) using cSLO showed characteristic signs of retinal degeneration with RPE irregularities visible in the native RF (513 nm, not shown), IR (830 nm), and AF modes (Fig. 3). SD-OCT imaging revealed a complete lack of ROS, whereas the ONL appeared only marginally thinner than the wild-type retina. Accordingly, central retinal thickness in *Rho*$^{-/-}$ mice was reduced to 193 ± 2 µm. The entire retina showed an absence of ROS, but the outer limiting membrane seemed not to be disturbed and could be distinguished from the RPE signal by a distance roughly equivalent to the extent of inner segment remnants (Fig. 3). Similarly, histologic sections showed an absence of ROS, whereas the outer nuclear layer appeared essentially intact with approximately six to eight rows of nuclei (Fig. 3).

Rpe65$^{-/-}$

Mutations in the gene encoding *RPE65* causes LCA2, a major form of Leber's congenital amaurosis,[25–27] which is targeted in current clinical gene therapy trials.[28,29] The protein RPE65 is expressed in the RPE, where it plays a pivotal role in maintaining normal vision by regenerating the visual pigment rhodopsin.[16] In *Rpe65*$^{-/-}$ mice, the blocked visual cycle causes an accumulation of retinyl esters in RPE cells, where they form large lipid droplets (Fig. 4A). Cone photoreceptors degenerate

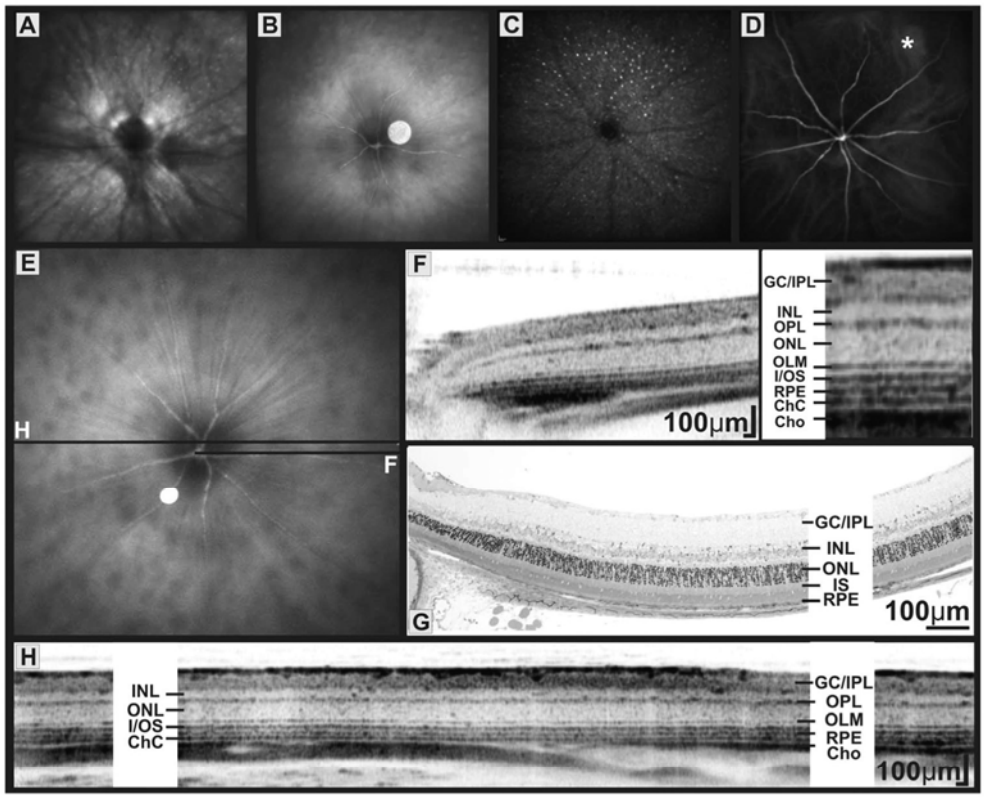

FIGURE 2. Retinal SLO imaging and OCT in BALB/c mice (PW10). Typical results of cSLO en face imaging in the presence of nonpigmented retinal structures in (**A**) native IR (830 nm), (**B**) RF (513 nm), and (**C**) AF modes. (**D**) Fluorescein angiography in BALB/c mice displayed both retinal and choroidal vasculature (*asterisk*) because lack of pigment allowed light at $\lambda = 488$ nm to better penetrate the RPE/choriocapillary complex. (**E**) Fundus image with indicated orientation (**F**, **H**) of corresponding B-scans. (**G**) Representative histologic data of an age-matched BALB/c mouse. (**H**) Virtual cross-section with designation of the different retinal layers. Note the altered signal composition in the outer retina because of the absence of pigmentation in BALB/c mice (**F**). There are four HRLs possibly demarcating the I/OS, RPE, nonpigmented choriocapillary, and choroidal structures. GC/IPL, ganglion cell/inner plexiform layer; OLM, outer limiting membrane; RPE/ChC, RPE/choriocapillary complex; Cho, choroid.

rapidly, whereas the remaining rods are the exclusive source of electrophysiological response and start to degenerate slowly only after approximately 6 months of age.[30,31] En face imaging at postnatal month (PM) 11 showed a characteristic pattern of hyperfluorescent flecks in the AF mode, which may again indicate metabolic remnants of photoreceptor outer segments (Fig. 4). Image resolution of SD-OCT in *Rpe65*$^{-/-}$ mice was insufficient to resolve intracellular lipid accumulations in vivo.

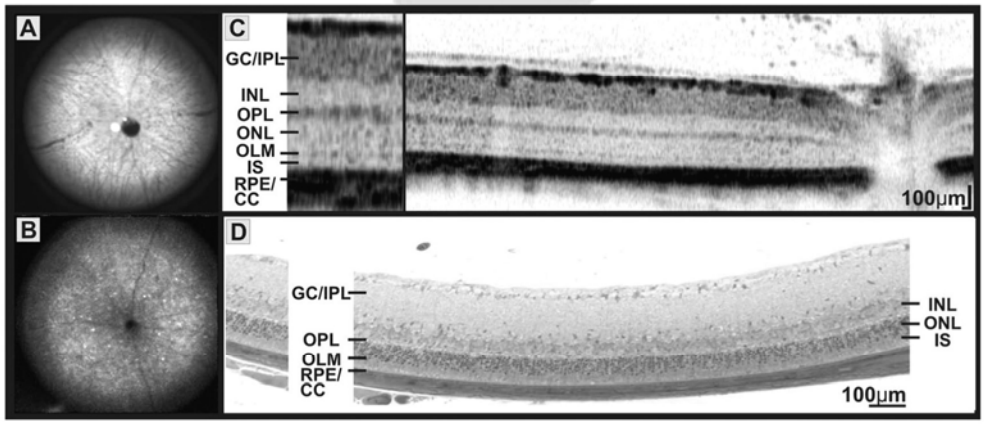

FIGURE 3. Retinal degeneration and RPE irregularities in the *Rbo*$^{-/-}$ mouse model (PW4). (**A**) Native IR (830 nm) and (**B**) AF mode cSLO data. (**C**) SD-OCT section and enlarged image, revealing a complete absence of ROS together with an apparent thinning of the ONL. (**D**) Ex vivo histology for comparison, confirming the observed reduction in ONL thickness and the lack of ROS. GC/IPL, ganglion cell/inner plexiform layer; OLM, outer limiting membrane; IS, photoreceptor inner segments; RPE/CC, RPE/choriocapillary complex.

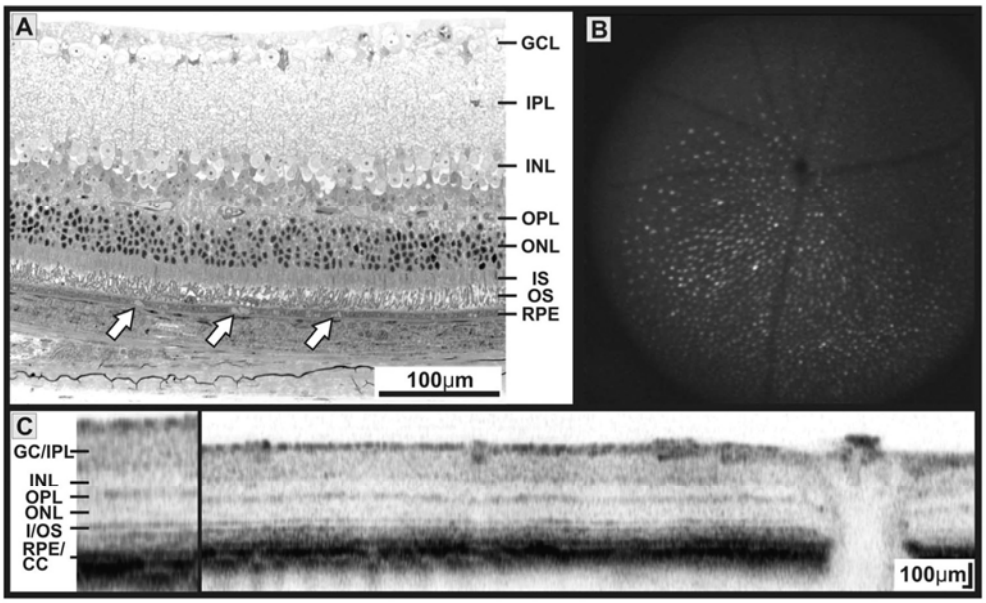

FIGURE 4. Retinal degeneration and RPE irregularities in the *Rpe65*$^{-/-}$ mouse model (PM11). (**A**) Histology showing lipid droplets from stored retinyl esters (*arrows*) in the RPE, together with a reduced retinal thickness. (**B**) Spots of hyperfluorescence in the AF mode, suggesting the presence of photoreceptor debris. (**C**) OCT cross-sectional image confirming a reduction of ONL thickness, though laminar organization (enlarged image) was not as clearly delineated as in wild-type mice. GC/IPL, ganglion cell/inner plexiform layer OLM, outer limiting membrane; RPE/CC, RPE/choriocapillary complex.

However, cross-sectional images revealed a reduction of ONL size, resulting in decreased total central retinal thickness of 193 ± 2 μm, which is more than the expected roughly 10% reduction with age and would be consistent with the observed AF.[32] Laminar organization in *Rpe65*$^{-/-}$ mice was not as clearly delineated, perhaps because of a generalized reaction to the ongoing photoreceptor loss. Indeed, it has been shown that the genetic response in *Rpe65*$^{-/-}$ mice includes modified expression of cytoskeletal elements and components of the extracellular matrix.[33] Such a global response might reasonably affect the optical characteristics of the retinal sublayers.

rd1

The autosomal recessive retinal degeneration in the *rd1* mouse is caused by a loss-of-function mutation in the gene encoding the β subunit of the rod cGMP phosphodiesterase 6 (PDE6β).[34] Numerous mutations in the catalytic domain of the human homolog, *PDE6β*, have been found in human patients with autosomal recessive retinitis pigmentosa (arRP).[35,36] Hence, the *rd1* mouse and other mouse strains harboring PDE6β mutant alleles are considered relevant animal models of retinitis pigmentosa.

First signs of rod photoreceptors cell loss in *rd1* mice become evident at approximately, P10 when looking at TUNEL stainings, whereas ONL reduction become evident at age P12 and P13 and most rod photoreceptor nuclei have disappeared by P21.[37,38] En face imaging in *rd1* mice at P11 failed to detect signs of retinal degeneration. In contrast, *rd1* mice at P28 revealed significant retinal degeneration both in the cSLO and SD-OCT imaging (Fig. 5). Cross-sectional images showed an intact inner retina, whereas the inner nuclear layer (INL) seemed to border the RPE almost directly with the OPL/ONL and photoreceptor segments virtually nonexistent. Although central retinal thickness in *rd1* at P28 showed a marked reduction to only 145 ± 5 μm, *rd1* mice at P11 featured a central retinal thickness at 246 ± 2 μm. The rapid progression of retinal degeneration in the *rd1* model has been analyzed before using a custom-made SD-OCT device.[5] This study adds to the published data by presenting the onset of retinal degeneration in this model and resolving the retinal architecture before photoreceptor cell death (P11).

SD-OCT versus Histology

Direct comparison of inner and outer retinal thickness assessed either by SD-OCT or histomorphometric analysis revealed excellent correlation (Figs. 6A–D). Consistent with existing data based largely on histologic assessment,[15,31,37] SD-OCT data revealed a significant reduction of the outer retinal thickness in *Rho*$^{-/-}$, *RPE65*$^{-/-}$, and BALB/c mice compared with C57/Bl6 animals (Fig. 6A). Similarly, timeline analysis of C3H wild-type versus C3H rd1/rd1 mice at P11 and P28 showed significant changes only in the rd1 mice at P28 (Fig. 6B). Traditional histomorphometric assessment mirrored the findings gained by SD-OCT data analysis (Fig. 6C), and direct comparison between the two data sets revealed excellent correlation coefficients for the whole retinal thickness (R^2 = 0.897) and outer retinal thickness, respectively (R^2 = 0.978). When analyzing the two data sets stemming from different protocols for histology separately (data not shown), the protocol using overnight fixation (*Rho*$^{-/-}$, *RPE65*$^{-/-}$, BALB/c, and C57/Bl6) featured the lower correlation coefficient (r^2 = 0.802) compared with the protocol using direct embedding, freezing, and sectioning (C3H wild-type and C3H rd1/rd1 mice at P11 and P28 [r^2 = 0.954]). This could arguably be attributed to differential shrinkage during processing for histology, and it highlights the benefit of noninvasive assessment of retinal thickness by SD-OCT.

DISCUSSION

OCT has emerged as a valuable tool to analyze and monitor structural changes in the retina. Although noninvasive in character, the resolution of cross-sectional images obtained by third-generation OCT begins to approach the level of low-power micrographs gained from light microscopy. This allows for detailed in vivo structural analysis of retinal disorders and

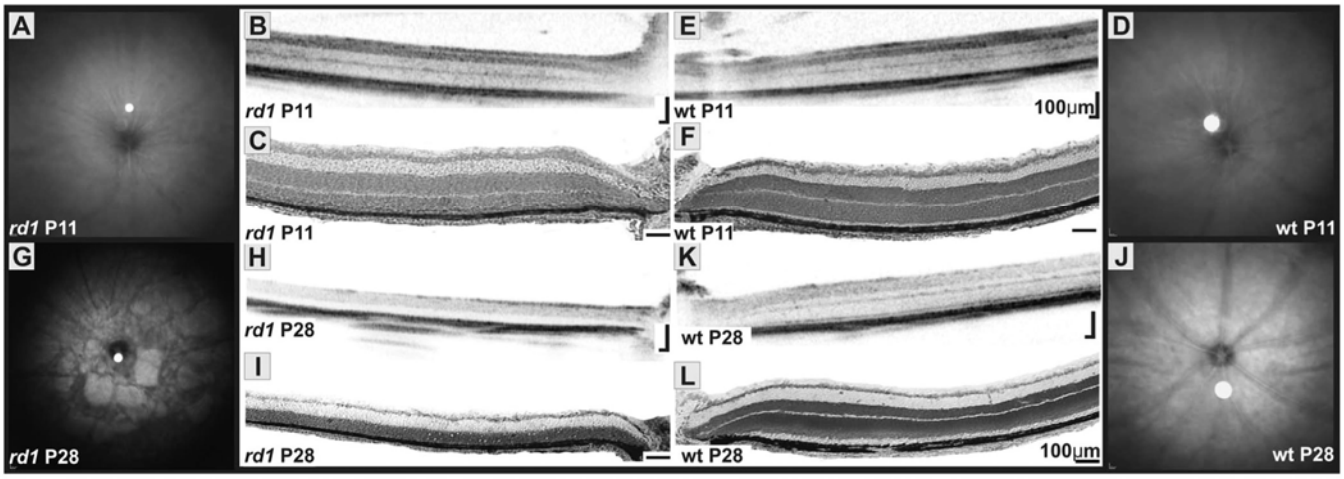

FIGURE 5. En face and SD-OCT imaging in *rd1* and corresponding wild-type control mice at P11 and P28. At P11, no signs of retinal degeneration were evident in (**A**, **D**) cSLO or (**B**, **E**) SD-OCT imaging. (**C**, **F**) Histology confirmed normal ONL thickness. In contrast, *rd1* mice at P28 revealed significant retinal degeneration (**G**). This pattern was also evident in the SD-OCT cross-sectional images (**H**) and corresponding histology (**I**), where inner retinal layers appeared intact, whereas the INL seemed to border the RPE almost directly. OPL/ONL and photoreceptor segments were virtually nonexistent. (**J**–**L**) Wild-type controls at P28 showed no signs of retinal degeneration. Scale bars, 100 μm.

bears importance for a refined genotype/phenotype correlation in a clinical setting and for noninvasive longitudinal studies on animal models that mimic respective disease characteristics. Indeed, various prototype OCT setups have been reported to allow noninvasive, high-resolution imaging of rodent retina.[6,7] Srinivasan et al.[7] used a custom build OCT setup to scan a normal C57/Bl6 mouse and to analyze the retinal thickness in a virtual cross-section obtained from a Long-Evans rat. Ruggeri et al.[6] demonstrated noninvasive retinal imaging (e.g., in a mouse model of retinal degeneration, $Rho^{-/-}$) using an experimental OCT system. Both studies compare single virtual cross-sections with conventional histology without quantification, whereas others have used custom OCT systems to monitor the dynamic changes of natural disease progression in respective animal models.[2,3,5] Yet the potential to evaluate therapeutic or adverse effects of experimental interventions in time-course experiments might prove to be even more important. Consequently, comparability between individual preclinical studies and preferably also between the preclinical and clinical setting will be of eminent importance. This is a challenge that is best addressed using commercially available equipment already approved for clinical use. In this study, we present data from frequently used wild-type mice and models of hereditary retinal degeneration using a commercially available third-generation OCT device approved for clinical diagnostic use.

The identity of signal composition in linear A- and two-dimensional B-scans acquired by OCT imaging has been subject to debate. However, it is generally thought[1,39,40] that—from vitreous to sclera—the first thin dark band resembles the nerve fiber layer followed by the lighter ganglion cell layer. The consecutive thick band of higher intensity illustrates the inner plexiform layer (IPL), approximated by a light band, the INL. The OPL appears as a thin stripe with signal intensity comparable to that of the IPL. The outer retina is composed of a thick light band, and ONL signal intensity is similar to that of INL. Apparently, both nuclear layers share the low signal intensity because they scatter or reflect light to a lesser extent than do both plexiform layers, which appear much darker. Located just distal to the ONL is the ELM, which is formed by adherence junctions between apical villi of Müller glia cells and distal photoreceptor cell bodies. Photoreceptor inner segments appear with the same signal intensity as the cell bodies, whereas the I/OS generates a strong signal possibly because of the high mitochondrial content in the ellipsoid region of the outer segment.[39] The photoreceptor outer segments are visible between the I/OS border and the equally strong signal of the RPE/choriocapillary complex. In pigmented retinas, choroidal structures cannot be reliably detected because light is almost completely scattered or reflected as it travels through the more proximal layers. In nonpigmented retinas, the signal composition is considerably different distal of the ELM (Fig. 2), which argues for scatter/reflection attributed to melanin granules as playing the main part in this phenomenon.

Earlier work exploring the correlation between OCT and histology in mice was performed primarily with second-generation, time-domain[2] or custom-made, high-resolution OCT devices[5] and reported a substantial overestimation of retinal thickness by OCT.[3] In this study we used a commercially available SD-OCT device and obtained high overall correlation of total retinal thickness (R^2 = 0.897) with only minor overestimation (2.5%) of retinal thickness by OCT. Interestingly, correlation of outer retinal thickness representing the photoreceptor cell layer separately showed an even higher Pearson's correlation coefficient (R^2 = 0.978, Fig. 6D). Overall, the results obtained in vivo are in good agreement with earlier studies on the three animal models for retinal degeneration.[15,31,37]

Although conventional histology features higher resolution, OCT delivers the advantage of producing morphologic data undistorted by handling, fixating, and staining procedures while being coregistered with en face topologic information. The latter aspect is particularly useful when assessing retinal degeneration types that do not show a uniform progression in the entire retina. OCT-based screening may also be useful for breeding purposes because it enables a noninvasive assessment of retinal health in mouse strains that are prone to develop sporadic retinal degeneration.

Analogous to electroretinography, by which the use of identical hardware in the clinical setting and laboratory has led to new insights,[31] the application of a clinically approved OCT device for animal studies bears the potential to translate insights from bench to bedside in an efficient and timely manner. Here, we present evidence on the efficacy of a commercially available SD-OCT in small animal retinal imaging and provide in vivo structural data on mouse models of retinal degeneration. This should facilitate further studies on dynamic changes of retinal structure through the natural course of disease and

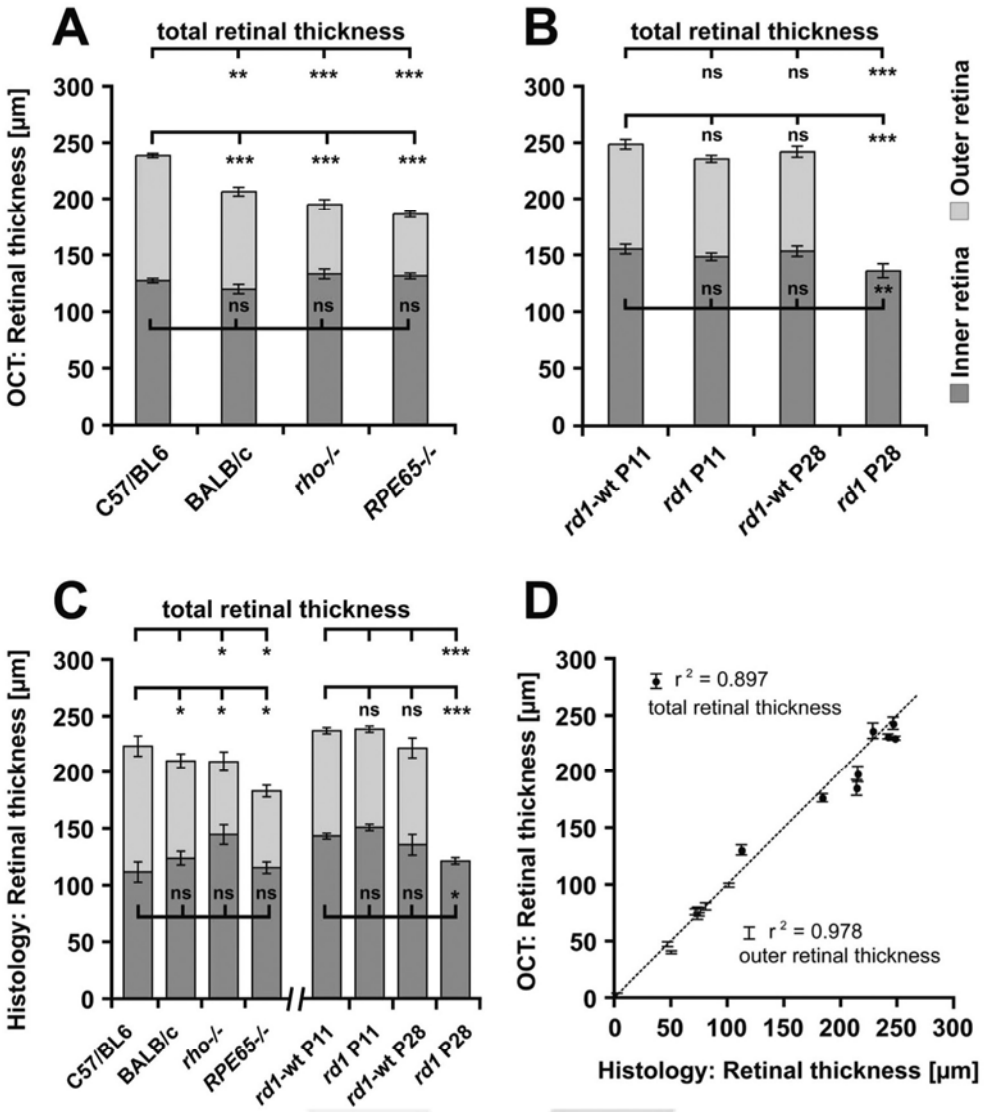

FIGURE 6. Evaluation of inner and outer retinal thickness in wild-type mice and animal models of hereditary retinal degeneration using either SD-OCT in vivo imaging or conventional morphometric assessment by histology. (**A–C**) Bar graphs indicate inner (*dark*) and outer (*light*) retinal thickness. (**A**) Note statistically significant reduction of outer but not inner retinal thickness in BALB/c, $Rho^{-/-}$ and $RPE65^{-/-}$ compared with C57/BL6 mice. (**B**) There is no statistical significant difference between *rd1* and wild-type mice at P11. Although outer retina remained unchanged in the wild-type mice at P28, there is complete loss of outer retina in the age-matched *rd1* mice. (**C**) Conventional morphometric assessment of retinal thickness in histologic sections with similar changes as reported by SD-OCT (**A**, **B**). Significance was calculated using Student's *t*-test. ns, not significant ($P > 0.01$); $^{*}P \leq 0.01$; $^{**}P \leq 0.001$; $^{***}P \leq 0.0001$. (**D**) Scatter plot shows the correlation of histologic versus OCT data on total (*dots*) and outer (*error bars* only) retinal thickness from C57/BL6, BALB/c, $Rho^{-/-}$, $RPE65^{-/-}$, *rd1-wt* P11, *rd1* P11, *rd1-wt* P28, and *rd1* P28 mice. Pearson's correlation coefficients (r^2) are displayed for total retinal thickness ($y = 0.975x$) and outer retinal thickness ($y = 1.018x$) separately. All data are reported as mean ± SD (*error bars*).

should help to monitor putative therapeutic effects of novel interventional strategies.

References

1. Drexler W, Fujimoto JG. State-of-the-art retinal optical coherence tomography. *Prog Retin Eye Res.* 2008;27:45–88.
2. Horio N, Kachi S, Hori K, et al. Progressive change of optical coherence tomography scans in retinal degeneration slow mice. *Arch Ophthalmol.* 2001;119:1329–1332.
3. Li Q, Timmers AM, Hunter K, et al. Noninvasive imaging by optical coherence tomography to monitor retinal degeneration in the mouse. *Invest Ophthalmol Vis Sci.* 2001;42:2981–2989.
4. Anger EM, Unterhuber A, Hermann B, et al. Ultrahigh resolution optical coherence tomography of the monkey fovea: identification of retinal sublayers by correlation with semithin histology sections. *Exp Eye Res.* 2004;78:1117–1125.
5. Kim KH, Puoris'haag M, Maguluri GN, et al. Monitoring mouse retinal degeneration with high-resolution spectral-domain optical coherence tomography. *J Vis.* 2008;17:1–11.
6. Ruggeri M, Wehbe H, Jiao S, et al. In vivo three-dimensional high-resolution imaging of rodent retina with spectral-domain optical coherence tomography. *Invest Ophthalmol Vis Sci.* 2007;48:1808–1814.
7. Srinivasan VJ, Ko TH, Wojtkowski M, et al. Noninvasive volumetric imaging and morphometry of the rodent retina with high-speed,

ultrahigh-resolution optical coherence tomography. *Invest Ophthalmol Vis Sci.* 2006;47:5522–5528.
8. Wolf-Schnurrbusch UE, Enzmann V, Brinkmann CK, Wolf S. Morphological changes in patients with geographic atrophy assessed with a novel spectral OCT-SLO combination. *Invest Ophthalmol Vis Sci.* 2008;49:3095–3099.
9. Chang B, Hawes NL, Hurd RE, Davisson MT, Nusinowitz S, Heckenlively JR. Retinal degeneration mutants in the mouse. *Vision Res.* 2002;42:517–525.
10. Seeliger MW, Beck SC, Pereyra-Munoz N, et al. In vivo confocal imaging of the retina in animal models using scanning laser ophthalmoscopy. *Vision Res.* 2005;45:3512–3519.
11. Buttery RG, Hinrichsen CF, Weller WL, Haight JR. How thick should a retina be? A comparative study of mammalian species with and without intraretinal vasculature. *Vision Res.* 1991;31:169–187.
12. Hanstede JG, Gerrits PO. The effects of embedding in water-soluble plastics on the final dimensions of liver sections. *J Microsc.* 1983;131:79–86.
13. O'Steen WK, Sweatt AJ, Eldridge JC, Brodish A. Gender and chronic stress effects on the neural retina of young and mid-aged Fischer-344 rats. *Neurobiol Aging.* 1987;8:449–455.
14. Chaudhuri A, Hallett PE, Parker JA. Aspheric curvatures, refractive indices and chromatic aberration for the rat eye. *Vision Res.* 1983;23:1351–1363.
15. Humphries MM, Rancourt D, Farrar GJ, et al. Retinopathy induced in mice by targeted disruption of the rhodopsin gene. *Nat Genet.* 1997;15:216–219.
16. Redmond TM, Yu S, Lee E, et al. Rpe65 is necessary for production of 11-cis-vitamin A in the retinal visual cycle. *Nat Genet.* 1998;20:344–351.
17. Frasson M, Picaud S, Leveillard T, et al. Glial cell line-derived neurotrophic factor induces histologic and functional protection of rod photoreceptors in the rd/rd mouse. *Invest Ophthalmol Vis Sci.* 1999;40:2724–2734.
18. Azadi S, Paquet-Durand F, Medstrand P, van Veen T, Ekstrom PA. Up-regulation and increased phosphorylation of protein kinase C (PKC) delta, mu and theta in the degenerating rd1 mouse retina. *Mol Cell Neurosci.* 2006;31:759–773.
19. Hauck SM, Ekstrom PA, Ahuja-Jensen P, et al. Differential modification of phosducin protein in degenerating rd1 retina is associated with constitutively active Ca2+/calmodulin kinase II in rod outer segments. *Mol Cell Proteomics.* 2006;5:324–336.
20. Samardzija M, Wenzel A, Aufenberg S, Thiersch M, Reme C, Grimm C. Differential role of Jak-STAT signaling in retinal degenerations. *FASEB J.* 2006;20:2411–2413.
21. Jaffe NS. The vitreous. *Arch Ophthalmol.* 1971;85:501–509.
22. Eisner G. [Postmortem slitlamp study of the vitreous body, II: pattern of vitreous structures made visible by the slitbeam]. *Albrecht Von Graefes Arch Klin Exp Ophthalmol.* 1971;182:8–22.
23. LaVail MM, Gorrin GM, Repaci MA. Strain differences in sensitivity to light-induced photoreceptor degeneration in albino mice. *Curr Eye Res.* 1987;6:825–834.
24. LaVail MM, Gorrin GM, Repaci MA, Thomas LA, Ginsberg HM. Genetic regulation of light damage to photoreceptors. *Invest Ophthalmol Vis Sci.* 1987;28:1043–1048.
25. Gu SM, Thompson DA, Srikumari CR, et al. Mutations in RPE65 cause autosomal recessive childhood-onset severe retinal dystrophy. *Nat Genet.* 1997;17:194–197.
26. Lorenz B, Gyurus P, Preising M, et al. Early-onset severe rod-cone dystrophy in young children with RPE65 mutations. *Invest Ophthalmol Vis Sci.* 2000;41:2735–2742.
27. Marlhens F, Bareil C, Griffoin JM, et al. Mutations in RPE65 cause Leber's congenital amaurosis. *Nat Genet.* 1997;17:139–141.
28. Bainbridge JW, Smith AJ, Barker SS, et al. Effect of gene therapy on visual function in Leber's congenital amaurosis. *N Engl J Med.* 2008;358:2231–2239.
29. Maguire AM, Simonelli F, Pierce EA, et al. Safety and efficacy of gene transfer for Leber's congenital amaurosis. *N Engl J Med.* 2008;358:2240–2248.
30. Rohrer B, Lohr HR, Humphries P, Redmond TM, Seeliger MW, Crouch RK. Cone opsin mislocalization in Rpe65$^{-/-}$ mice: a defect that can be corrected by 11-cis retinal. *Invest Ophthalmol Vis Sci.* 2005;46:3876–3882.
31. Seeliger MW, Grimm C, Stahlberg F, et al. New views on RPE65 deficiency: the rod system is the source of vision in a mouse model of Leber congenital amaurosis. *Nat Genet.* 2001;29:70–74.
32. Gresh J, Goletz PW, Crouch RK, Rohrer B. Structure-function analysis of rods and cones in juvenile, adult, and aged C57BL/6 and Balb/c mice. *Vis Neurosci.* 2003;20:211–220.
33. Cottet S, Michaut L, Boisset G, Schlecht U, Gehring W, Schorderet DF. Biological characterization of gene response in Rpe65$^{-/-}$ mouse model of Leber's congenital amaurosis during progression of the disease. *FASEB J.* 2006;20:2036–2049.
34. Bowes C, Li T, Danciger M, Baxter LC, Applebury ML, Farber DB. Retinal degeneration in the rd mouse is caused by a defect in the beta subunit of rod cGMP-phosphodiesterase. *Nature.* 1990;347:677–680.
35. McLaughlin ME, Ehrhart TL, Berson EL, Dryja TP. Mutation spectrum of the gene encoding the beta subunit of rod phosphodiesterase among patients with autosomal recessive retinitis pigmentosa. *Proc Natl Acad Sci U S A.* 1995;92:3249–3253.
36. McLaughlin ME, Sandberg MA, Berson EL, Dryja TP. Recessive mutations in the gene encoding the beta-subunit of rod phosphodiesterase in patients with retinitis pigmentosa. *Nat Genet.* 1993;4:130–134.
37. Paquet-Durand F, Silva J, Talukdar T, et al. Excessive activation of poly(ADP-ribose) polymerase contributes to inherited photoreceptor degeneration in the retinal degeneration 1 mouse. *J Neurosci.* 2007;27:10311–10319.
38. Sancho-Pelluz J, Arango-Gonzalez B, Kustermann S, et al. Photoreceptor cell death mechanisms in inherited retinal degeneration. *Mol Neurobiol.* 2008;38:253–269.
39. Fischer MD, Fleischhauer JC, Gillies MC, Sutter FK, Helbig H, Barthelmes D. A new method to monitor visual field defects caused by photoreceptor degeneration by quantitative optical coherence tomography. *Invest Ophthalmol Vis Sci.* 2008;49:3617–3621.
40. Srinivasan VJ, Monson BK, Wojtkowski M, et al. Characterization of outer retinal morphology with high-speed, ultrahigh-resolution optical coherence tomography. *Invest Ophthalmol Vis Sci.* 2008;49:1571–1579.

V. DISCUSSION AND FUTURE PROSPECTS

Animal studies in retinal degenerations are important to gain a deeper understanding of the pathophysiology of the corresponding human diseases and the development of treatment strategies. In inherited forms, mouse models are particularly valuable due to the opportunity to knock out respective causative genes (Takahashi et al. 1994, Kim et al. 2008). Over the past decade, many such knock out mice have been generated to study a variety of retinal degenerative diseases (Chang et al. 2002, Wu et al. 2004), and several more are being developed. They have also proven to be useful in the assessment of treatment options such as gene and stem cell therapy. Consequently, the number of studies on disease progression and therapeutical approaches is rising.

However, it has been difficult to analyze and quantify retinal morphology and anatomy of the rodent retina without sacrificing the animal for conventional histology. In most cases, cross-sectional studies are performed to elucidate biological features, i.e. they are based on data from animal models sacrificed at different time points. This has the disadvantage that there is no information about intermediate periods, and that the animals used at one time point may systematically differ from that at another (e.g. due to breeding, food quality and intake, seasonal issues, number of siblings, temperature, light (cage position)). Because biological processes are subject to permanent modifications and alterations, the possibility of dynamic and systematic studies would promote a more comprehensive picture of the process. The key issue is that changes in retinal morphology could so far not be followed noninvasively during the course of degeneration in an individual animal; therefore, each animal contributed to just one single time point, and all other information about the actual disease progression in this individual was lost. It is well known that such cross-sectional studies are statistically inferior to longitudinal studies because of the higher impact of interindividual variability. Consequently, larger numbers of animals must be sacrificed during the evaluation of disease progression to obtain statistically significant experimental results (Li et al. 2001).

Numerous efforts of *in vivo* imaging in animals, particularly in rodents, have been made, but the visualization of the rodent retina has been challenging due to the small pupil size, short focal length, and thin retina (Srinivasan et al. 2006). Recently, the OCT has also been introduced as a new tool for the *in vivo* analysis of rodent eyes

(Ruggeri et al. 2007, Ko et al. 2004, Kim et al. 2006). Because previous commercially available first and second generation OCT devices based on time-domain technology lacked sufficient image quality to asses retinal morphology in small animals (Horio et al. 2001, Li et al. 2001), several prototype devices were built (Anger et al. 2004, Kim et al. 2008, Ruggeri et al. 2007). These custom-made OCT setups were specifically adapted for each respective animal visual system, but have not been made in sufficiently large numbers to have an impact on the scientific community. A further, unresolved issue is that morphometric results generated with different OCT setups varied significantly in dimensions. Only recently, third generation OCT devices providing major scanning speed and depth-resolution advantages compared to time-domain devices became commercially available (Wolf-Schnurrbusch et al. 2008).

In this study, a commercially available third generation OCT device (Spectralis HRA+OCT® Heidelberg Engineering, Heidelberg, Germany) was adapted to the optical properties of the murine eye. Compared to first and second generation devices, it provides improved performance with regard to parameters like scanning speed and depth resolution, the latter being crucial for the use in rodent eyes. As Podoleanu (1997, 1998) already mentioned, the combination of SLO and OCT offers the possibility to combine en face and cross-sectional images to add complementary information. It is however also important to be able to locate sites of interest for a more detailed inspection with OCT, in particular in the presence of solitary lesions, as shown in the first included manuscript (Fischer et al. 2009), where nature and extent of such solitary lesions were examined.

In this work, the substantial methodological challenges of *in vivo* imaging in rodent eyes have been overcome without internal modification of the commercial setup by mounting a commercially available ophthalmologic standard Volk 78 dpt. ophthalmoscopic lens directly in front of the camera unit. This simplifies the optical design, reduces aberrations and provides a reasonably wide field of view for OCT scanning.

Poor optical media due to cataract, corneal scarring, or vitreous opacities are the main limitations encountered in *in vivo* imaging in rodents. Corneal transparency is one of the keys for high-quality OCT images. To avoid media opacities under anesthesia, a plastic contact lens was fixed onto the cornea by a drop of methylcellulose 2% to prevent the cornea from drying out.

To prevent image artifacts during OCT recording due to body movements (e.g. caused by breathing), an image alignment software (TruTrack™) was used that

continuously monitors the position of image landmarks like vessels and the optic disc and accordingly corrects the position of the area used for averaging.

Very important for the scientific community is the consistency of results between different studies. The use of commercially available equipment to perform imaging in small animals bears the possibility to enhance the worldwide comparability of results, and generates reliable and reproducible results that compare well to histological cross-sections. In terms of availability, reproducibility, familiarization and standardization, commercial setups are therefore superior to custom-made ones and particularly valuable for the future spread of this technique.

OCT imaging has also important functional advantages over conventional imaging techniques and standard histology. Ultrahigh resolution time-domain OCT systems provide unique information about ocular structures *in vivo*, which, like edema formation, were previously not even accessible by means of histology (Fischer et al. 2009). Because OCT is noninvasive, the same specimen can be monitored over a prolonged period to observe changes in morphology in the same animal, which allows to follow up the degenerative changes or therapeutical approaches over time.

Similar to ultrahigh-resolution imaging in the human retina, imaging in the murine retina enables visualization of major intraretinal layers (Drexler et al. 2003, Ko et al. 2004). However, the data arising from a novel imaging technology also create the need for a proper interpretation. The OCT is no exception in this respect, and the lack of an appropriate gold standard makes this task not easier. In contrast to histology, the optical path in OCT is from top to bottom of the image, which leads to windowing effects (i.e. structures behind strongly reflective ones are less well visible), and potential distortion due to variations in optical properties from layer to layer. However, a comparison with histological images taken of the same identical eye has shown that these potential problems apparently do not play a major role in the interpretation of OCT images of the murine retina. An exception is the distal outer retina, where the classification of reflecting bands is still challenging.

It is important to note that OCT is capable to resolve reflectance changes induced by tissue optical scattering properties and refractive index discontinuities, but it cannot distinguish between tissues of similar optical properties (Srinivasan et al. 2006). By comparison, histology visualizes tissues by light absorbance according to specific staining properties (Toth et al. 1997). Although OCT does not yet allow a resolution of the retina at a cellular level, it is possible to track morphologic alterations in retinal diseases *in vivo*, like the site of edema in light damage models (Fischer et al. 2009).

Whereas the reflectivity profiles of the proximal part of the retina, ranging from the internal limiting membrane to the junction of the inner and outer segments of the photoreceptor layer, are widely congruent with histology (Anger et al. 2004, Gloesmann et al. 2003), the origin of signals arising from the distal part of the outer retina, including the retinal pigment epithelium (RPE), Bruch`s membrane, choriocapillaris, and the choroidal complex, has been subject to debate. Recently, the current opinion about the cellular basis of these reflectivity profiles has been summarized (Huber et al. in press).

Anger (2004) pointed out that a quantitative comparison of OCT images to histology may be difficult because of histologic processing artifacts, such as nonlinear tissue shrinkage, depending on the applied fixation protocols. Since OCT is an *in vivo* technique, it reflects tissue dimensions under live conditions. The morphologic data generated by OCT therefore is not influenced by changes in tissue structure associated with handling, fixating and staining procedures.

In contrast to former studies (Horio et al. 2001, Li et al. 2001, Kim et al. 2008) it could be shown in the present work that the overall retinal thickness was only marginally overestimated compared to histology (Huber et al. in press). Besides, no significant differences in layer thickness were detectable between the two methods (Fischer et al. 2009). Retinal detachments are also difficult to assess with histological means, as their extent may be altered by tissue processing, and sometimes they even form postmortem. In contrast, OCT scans provide a more realistic estimate of their structure and dimensions. The visualization of retinal detachments is extremely important not only for the assessment of structural alterations associated with diseases, but also for evaluation and follow-up of subretinal surgical procedures. The evaluation of the success of subretinal manipulations and the injection of therapeutic and/or experimental reagents like in gene therapy is thus an important field of application of the OCT.

The OCT has opened new avenues for visualizing and recording over time dynamic changes in genetic, developmental and disease mechanisms that cannot be captured by conventional light microscopy (Farkas and Becker 2001). A practical advantage is that OCT scanning and image acquisition is very fast and relatively inexpensive, and results can be obtained easily from a large number of animals within a period comparing very favorably to lengthy histological procedures.

Given the variety of new gene and pharmacologic therapies that may cure or retard the progression of retinal degenerations (Ali et al. 1997, Benett et al. 1996, Lewin et

al. 1998, LaVail et al. 1998, Hauswirth and Timmers 2000), the ability to observe a therapeutic regimen through its entire course in individual rodent models greatly enhances the reliability and speed of testing, and would help to reduce the number of experimental animals needed. In analogy to electroretinography (ERG), where translational research using identical hardware in clinical and experimental settings resulted in adaptation of standard ERG protocols (Marmor and Zrenner 1993) and new insights in ERG signal composition (Seeliger et al. 2001), one might expect a similar impact of SD-OCT as it is readily available in patient care. In addition, the use of identical systems allows a direct comparison of retinal images acquired in a mouse model of a specific ocular disease or condition with images obtained clinically in human subjects (Kocaoglu et al. 2007). Furthermore, OCT images are in digital form and therefore are inherently quantifiable for statistical analysis. Finally, standard-ERG analysis and OCT imaging can be performed sequentially in the same animal, thus allowing essentially simultaneous documentation of retinal function and structure in the same living animal.

The growing number of newly established mouse models which feature genetically based retinal degeneration (Frederick et al. 2000, Petersen-Jones 1998) has increased the need for informative and efficient animal experiments. There is an urge for a rapid, noninvasive analysis of retinal degeneration in mouse eyes, for that the number of animal needed for experiments is not getting out of hand.

For the scientific community, there are different reasons to replace animal testing whenever and wherever possible. Animal welfare is an important consideration that is strongly backed by scientific, economic, logistical, ethical, legal and political pressures. Similarly compelling is the development of better, scientifically more advanced methods for a subsequent use in humans. In addition, alternative methods in general tend to be less expensive to perform, and, more important, to have a higher rate of test item throughput. A most satisfying aspect is that both humans and animals are expected to benefit from this work (Balls 2002).

A convenient and standardized way to objectively assess animal pain and distress is difficult to establish. This assessment is rather based on subjective clinical signs of abnormal behaviour and appearance. Because proper evaluation of pain relies largely on the ability to understand the behaviour and needs (Fraser and Broom 1990) of each species of laboratory animals, it is most suitable for investigators to assume that a procedure which inflicts pain and distress in humans will inflict at least as much pain and distress in animals unless there is evidence to the contrary

(Goldberg et al. 1996).

Russel and Burch (1959) published their considerations concerning the humane treatment of laboratory animals half a century ago. The development of various genetically modified strains more than ever emphasizes the need for alternative methods in animal experimentation. Focusing on the three R`s, recently developed noninvasive imaging methods contribute not only to replacement and refinement but also have the power to reduce the absolute number of animals needed due to the possibility of follow-up studies on almost arbitrary time points in the very same individual. Furthermore, the successful application of a commercially available tool renders the possibility to achieve worldwide standardization and assignability of both technical features as well as standardized examination protocols. This will increase the degree of acceptance and the number of diversified applications due to benefits for researchers in charge. Standardized examination protocols and features facilitate a replacement of check-up studies due to establishment of norm values of frequently used control animals at various ages. A lower number of animals implies not only fewer costs, but, even more important when it comes to thinking about animal welfare, should be the possibility to visualize the condition of each eye of every single animal at every chosen time point. Thus, OCT has the potential to reduce distress and pain in laboratory animals because morphological changes caused by retinal degeneration or adverse effects of therapeutical approaches are visible within time, which enables a gentle withdrawal of experiments at an early stage.

In the last two decades, technical advances and new experimental animal models gave privileged insight into specific aspects of retinal morphology. Moreover, the unique features of OCT will enable a broad range of new research and clinical applications in the future that will not only complement existing imaging technologies available today, but also will reveal new and previously invisible morphological, dynamic and functional changes in the retina (Drexler and Fujimoto 2008).

It is well known that changes in blood flow and vascularization are early precursors of important diseases such as diabetes (Leitgeb 2007). In analogy to ultrasound, a logical step is to retrieve blood flow information from the additional Doppler shifts induced by moving blood in the retinal vasculature (Yazdanfar et al. 2003).

New dimensions have been added, like measuring tissue oxygenation based on spectroscopy (Faber et al. 2004), or observing physiological responses within the retina (Bizheba et al. 2006). Furthermore, polarization-sensitive OCT uses the birefringent characteristics of the retinal nerve fiber layer and the RPE to better

assess their thickness (Cense et al. 2002, Pircher et al. 2004). Other functionalities will become available if shown to be useful. Very promising are the developments in contrast-enhanced molecular optical imaging, for example with the use of contrast agents targeted at specific tissue or cell structures. Functional OCT promises not only to improve image contrast, but also to enable the differentiation and early detection of pathologies by using integrated structural and functional imaging. These technological advances suggest that OCT will ultimately provide visualization of tissue morphology at a cellular level, thus enabling optical biopsies while imaging metabolic and physiological processes, in one single volumetric OCT measurement (Drexler and Fujimoto 2008).

Despite the fact that many of the functional OCT options mentioned above show great potential, it is unlikely that one machine will be able to provide all these modalities. Besides, interpretation of the results of these new implementations will require extensive experience.

In conclusion, as OCT devices become more and more elaborated, one may expect a diversification of capabilities and techniques such as Doppler flow, polarization-sensitive OCT, or depth-resolved functional imaging promising to integrate structural and functional information into a single measurement. OCT thus holds the promise for continuing advances in fundamental research and improvements in clinical care.

VI. SUMMARY

Noninvasive assessment of retinal morphology in mice using optical coherence tomography

In comparison to other organs, the eye is ideally suited for examination with imaging techniques because ocular media are essentially transparent. They transmit light with only minimal optical attenuation and scattering and provide excellent optical access to the retina.

Animal models are indispensable tools for understanding the cellular and molecular events associated with human retinal degenerative diseases. This is because functional and histological data of human patients are mostly available from advanced cases, and due to the slow progression of degenerative processes, it is rarely possible to do follow-up studies within a reasonable amount of time and trustworthy results.

As most inherited retinal degenerations are monogenic, the majority of studies focuses on genetically modified mice replicating the human disorder. It is anticipated that the already substantial number of studies on the rodent visual system will further grow with the rapid developments of novel genetic, biomedical, and physiological tools. Since there is, up to now, no curative treatment for these potentially blinding diseases, research on animal models is the basis for the understanding of the underlying pathophysiology and the development and assessment of therapeutical strategies.

Until today, the gold standard for analyzing the structural component of retinal pathophysiology including the assessment of disease progression and the evaluation of therapeutical approaches is histological examination. As a result, large numbers of animals must be sacrificed to obtain statistically significant experimental results for each time point included.

In this work, optical coherence tomography (OCT) was implemented to obtain histology-like images of retinal structure in live mice. For the first time, a commercially available high-resolution third generation OCT designed for use in human patients (Spectralis HRA+OCT®, Heidelberg Engineering, Heidelberg, Germany) was adapted for *in vivo* imaging in rodents. The associated methodological challenges have been overcome without the need for an internal modification of the commercial setup.

The successful application of a commercially available tool renders the possibility to achieve international standardization and assignability of both technical features as well as examination protocols. Such standards will also remove the need for individual studies to establish norm values in frequently used control strains at various ages. The expected replacement of conventional histological sections and the potential to conduct follow-up studies will almost certainly lead to a significant reduction of animals needed. In individual experimental animals, OCT further has the potential to reduce distress and pain because morphological changes caused by retinal degeneration or adverse effects of therapeutical approaches become visible as early as they occur, which enables a termination of experiments at that stage (refinement). Taken together, it is expected that these benefits of the OCT will help to increase the acceptance of the inevitable animal experiments in retinal degeneration research in the future.

VII. ZUSAMMENFASSUNG

Nicht-invasive Beurteilung der Netzhautmorphologie bei Mäusen mittels optischer Kohärenztomographie

Das Auge eignet sich im Gegensatz zu anderen Organen aufgrund der Lichtdurchlässigkeit optischer Medien besonders gut für die Untersuchung mit bildgebenden Verfahren.

Für die effektive Aufklärung der pathophysiologischen Grundlagen und der Bewertung von Therapieverfahren für menschliche erbliche Netzhautdegenerationen ist die Forschung an Tiermodellen Grundvoraussetzung. Funktionelle und histologische Daten beim Menschen liegen meist nur von fortgeschrittenen Krankheitsstadien vor. Auch Verlaufsuntersuchungen sind durch den langsamen Degenerationsprozess in überschaubaren Zeiträumen nicht oder nur unzuverlässig möglich.

Die steigende Zahl bekannter Gene und die breite Etablierung der Techniken zur Generierung von Mausmodellen führen zu einer stetig steigenden Anzahl von Mausmutanten, was wiederum zu einem konstanten Anstieg der Forschungsprojekte führt.

Als derzeitiger Goldstandard der Analyse retinaler Pathophysiologien allgemein als auch über Zeitverlauf von Degeneration und Effekten von Therapiestrategien im Besonderen gilt die histologische Untersuchung. Zu jedem Untersuchungszeitpunkt muss hierfür eine bestimmte Anzahl an Tieren euthanasiert werden, um statistisch aussagekräftige Daten zu erhalten.

Im Rahmen dieser Arbeit wurde nun erstmalig ein kommerziell verfügbares Basisgerät aus der Humandiagnostik (Spectralis HRA+OCT®, Heidelberg Engineering, Heidelberg, Deutschland) zur *in vivo* Darstellung der Retina bei Mäusen eingesetzt. Die erfolgreiche Adaption des Humangerätes an die optischen Eigenschaften des Mausauges konnte ohne Eingriffe in das Setup durchgeführt werden. Der hochauflösende optische Kohärenztomograph liefert dem Untersucher routinemäßig Bilder der Netzhaut in bisher nicht erreichter Qualität.

Die erfolgreiche Adaption eines kommerziell verfügbaren Gerätes ermöglicht eine weltweite Standardisierung der Untersuchungsprotokolle und damit eine Übertragbarkeit der Daten. Durch die Erstellung mauslinienspezifischer Normwerte

kann das OCT zum *replacement* durch den Ersatz von Kontrolluntersuchungen beitragen. Die histologieäquivalente Auflösung retinaler Strukturen und Verlaufsuntersuchungen an ein und demselben Individuum ermöglichen eine Reduktion (*reduction*) der Tierzahlen durch den Ersatz konventioneller Histologie. Des Weiteren ermöglicht das OCT ein zeitnahes Erkennen belastender pathologischer Veränderungen und eventueller Nebenwirkungen bei der Therapieentwicklung, so dass durch frühzeitigen Versuchsabbruch eine potentielle Verminderung der Belastung (r*efinement*) der Versuchstiere gegeben ist.

Diese Vorteile der *in vivo* Darstellung retinaler Strukturen lassen auf eine hohe Akzeptanz und eine breite Anwendung des OCTs in der Zukunft hoffen.

VIII. LIST OF REFERENCES

A

Ali RR, Reichel MB, Hunt DM, Bhattacharya SS: Gene therapy for inherited retinal degeneration. Br J Ophthalmol 1997;81:795-801

Anger EM, Unterhuber A, Hermann B, Sattmann H, Schubert C, Morgan JE, Cowey A, Ahnelt PK, Drexler W: Ultrahigh resolution optical coherence tomography of the monkey fovea: identification of retinal sublayers by correlation with semithin histology sections. Exp Eye Res 2004; 78:1117-1125

Animal Welfare Act as Amended (7 USC, 2131-2159) Government Printing Office

ARVO Statement for the Use of Animals in Ophthalmic and Visual Research 2009, see: http://www.arvo.org/eweb/dynamicpage.aspx?site=arvo2&webcode=AnimalsResearch

B

Balls M: Alternatives to animal experimentation. Alternatives to Laboratory Animals 1983;11:56-62

Balls M: Future Improvements: Replacement in Vitro Methods. ILAR Journal 2002; 43:69-73

Benett J, Tanabe T, Sun D: Photoreceptor cell rescue in retinal degeneration (rd) mice by in vivo gene therapy. Nat Med 1996; 2:649-654

Bizheba K, Pflug R, Hermann B, Povazay B, Sattmann H, Qiu P, Anger E, Reitsamer H, Popov S, Taylor JR, Unterhuber A, Ahnelt P, Drexler W: Optophysiology: depth-resolved probing of retinal physiology with functional ultrahigh-resolution optical coherence tomography. Proc Natl Acad Sci USA 2006; 103:5066-5071

Bok D: The retinal pigment epithelium: a versatile partner of vision. J Cell Sci 1993; Sup.17:189-195

Born M, Wolf E, Bhatia AB: Principles of Optics: Electromagnetic Theory of Propagation, Interference and Diffraction of Light. 7th (expanded) ed. Cambridge, England: Cambridge University Press; 1999

Boulton M, Dayhaw-Barker P: The role of the retinal pigment epithelium: topographical variations and ageing changes. Eye 2001; 15:384-389

Bunt-Milham AH, Saari JC, Klock IB, Gerwin GG: Zonulae adherens pore size in the external limiting membrane of the rabbit retina. Invest Ophthalmol Vis Sci. 1985; 26:1377-80

C

Cajal SR: The Structure of the Retina. Thomas, Springfield, 1972

Cense B, Chen TC, Park BH, Pierce MC, de Boer JF: In vivo depth-resolved birefringence measurements of the human retinal nerve fiber layer by polarization-sensitive optical coherence tomography. Opt Lett 2002; 27:1610-1612

Cense B, Nassif NA, Chen TC, Pierce MC, Yun SH, Park BH: Ultrahigh-resolution high-speed retinal imaging using spectral-domain optical coherence tomography. Optics Express 2004; 12:2435-2447

Chang B, Hawes NL, Hurd RE, Davisson MT, Nusinowitz S, Heckenlively JR: Retinal degeneration mutants in the mouse. Vision Research 2002; 42:517-525

Connolly SE, Hores TA, Smith LE, D`Amore PA: Characterization of vascular development in the mouse retina. Microvasc. Res. 1988; 36:275-290

Council Directive 86/609/EEC of 24 November 1986 on the approximation of laws, regulations and administrative provisions of the Member States regarding the protection of animals used for experimental and other scientific purposes

Curcio CA, Sloan KR Jr, Packer O, Hendrickson AE, Kalina RE: Distribution of cones in human and monkey retina: individual variability and radial asymmetry. Science. 1987; 236(4801):579-82

Cuthbertson RA, Mandel TE: Anatomy of the mouse retina. Endothelial cell-pericyte ratio and capillary distribution. IOVS 1986; 27(11):1659-1664

D

de Boer JF, Cense B, Park BH, Pierce MC, Tearney GJ, Bouma BE: Improved signal-to-noise ratio in spectral-domain compared with time-domain optical coherence tomography. Opt Lett 2003; 28:2067-2069

Detwiler SR: Vertebrate Photoreceptors. 1943, Macmillan, New York

Detwiler SR: The Eye and its structural Adaptations. Proceedings of the American Philosophical Society 1955; 99(4):224-238

Drexler W, Morgner U, Ghanta RK, Kärtner FX, Schuman JS, Fujimoto JG: Ultrahigh-resolution ophthalmic optical coherence tomography. NatMed 2001;7:502-507

Drexler W, Sattmann H, Hermann B, Ko TH, Stur M, Unterhuber A, Scholda C, Findl O, Wirtitsch M, Fujimoto JG, Fercher AF: Enhanced Visualization of Macular Pathology with the use of ultrahigh-resolution optical coherence tomography. Arch Ophthalmol. 2003; 121:695-706

Drexler W, Fujimoto JG: State-of-the-art retinal optical coherence tomography. Prog Ret Eye Research 2008; 27:45-88

F

Faber DJ, Aalders MCG, Mik EG, Hooper BA, van Gemert MJC, van Leeuwen TG: Oxygen saturation-dependent absorption and scattering of blood. Phys Rev Lett 2004; 93, 028102

Farber DB, Flannery JG, Bowes C: The rd mouse story: seventy years of research on an animal model of inherited retinal degeneration. Prog Ret Eye Res 1994;13:31-64

Farkas DL, Becker D: Applications of Spectral Imaging: Detection and Analysis of Human Melanoma and Its Precursors. Pigment Cell Res 2001; 14:2-8

Fercher AF, Mengedoht K: Werner W Eye-length measurement by interferometry with partially coherent light. Optics Letters 1988; 13:1867-1869

Fercher AF, Hitzenberger CK, Drexler W, Kamp G, Sattmann H: In vivo Optical Coherence Tomography. American Journal of Ophthalmology 1993; 116(1):113-115

Fercher AF, Hitzenberger CK, Kamp G, El-Zaiat SY: Measurement of intraocular distances by backscattering spectral interferometry. Opt Commun 1995; 117:43-48

Fischer MD, Huber G, Beck SC, Tanimoto N, Muehlfriedel R, Fahl E, Grimm C, Wenzel A, Remé CE, van de Pavert SA, Wijnholds J, Pacal M, Bremner R, Seeliger MW: Noninvasive, in vivo assessment of mouse retinal structure using optical coherence tomography. PLoS ONE 2009

Flecknell PA: Refinement of Animal Use - assessment and alleviation of pain and distress. Laboratory Animals 1994; 28(3):222-231

Fraser D, Brom DM: Farm animal behaviour and welfare. 1990 Wallingford, CAB International

Frederick J, Bronson JD, Baehr W: Animal models of inherited retinal diseases. Methods Enzymol. 2000; 316:515-526

Fujimoto JG: Optical coherence tomography for ultrahigh resolution in vivo imaging. Nature Biotechnology 2003; 21(11):1361-1367

Fujimoto JG, Brezinski ME, Tearney GJ: Optical biopsy and imaging using optical coherence tomography. Nature Med 1995; 1:970-972

Fujimoto JG, Pitris C, Boppart SA, Brezinski ME: Optical coherence tomography: an emerging technology for biomedical imaging and optical biopsy. Neoplasia 2000; 2(12):9-25

Futter CE, Ramalho JS, Jaissle GB, Seeliger MW, Seabra, MC: The role of Rab27a in the Regulation of Melanosome Distribution within Retinal Pigment Epithelial Cells. Molecular Biology of the Cell 2004; 15:2264-2275

G

Gloesmann M, Hermann B, Schubert C, Sattmann H, Ahnelt PK, Drexler W: Histologic correlation of pig retina radial stratification with ultrahigh-resolution optical coherence tomography. Ophthalmol Vis Sci 2003; 44:1696-3

Goldberg AM, Locke PA: To 3R is Humane. The Environmental Forum 2004; 6:19-26

Goldberg AM, Zurlo J, Rudacille D: The Three Rs and Biomedical Research. Science 1996;272(5267):1403-0

Graw J: The Genetic and Molecular Basis of Congenital Eye Defects. Nature 2003; 4:876-888

Grieve KF, Dubois A, Boccara C, Sahel J, Paques M, Picaud S, Le Gargasson JF: High–Speed Ultrahigh–Resolution Full–Field Optical Coherence Tomography: Application to Anterior Segment Imaging in Rats. IOVS 2005; 46:E-Abstract 2564

H

Hauswirth WW, Timmers AM: The eyes have it. Mol Med Today 2000;6:51-53

Heckenlively JR, Arden GB: Principles and practice of clinical electrophysiology of vision. 2nd edition 2006, Massachusetts Institute of Technology, Cambridge

Hee MR, Izatt JA, Swanson EA, Huang D, Schuman JS, Lin CP, Puliafito CA, Fujimoto JG: Optical Coherence Tomography of the Human Retina. Arch Ophthalmol. 1995; 113:325-332

Hee MR, Baumal CR, Puliafito CA, Duker JS, Reichel E, Wilkins JR, Coker JG, Schuman JS, Swanson EA, Fujimoto JG: Optical Coherence Tomography of age-related macular degeneration and choroidal neovascularization. Ophthalmology. 1996;103(8):1260-70

Hee MR, Puliafito CA, Duker JS, Reichel E, Coker JG, Wilkins JR, Schuman JS, Swanson EA, Fujimoto JG: Topography of diabetic macular edema with optical coherence tomography. Ophthalmology 1998; 105(2):360-370

Heidelberg Engineering available at: http://www.heidelbergengineering.com/products/spectralis-hra-oct/

Helb HM, Charbel Issa P, Fleckenstein M, Meyer CH, Holz FG: Clinical evaluation of simultaneous confocal scanning laser ophthalmoscopy imaging combined with high-resolution, spectral-domain optical coherence tomography. Acta Ophthalmologica 2009; 87:in press

Hitzenberger CK: Measurement of corneal thickness by low-coherence interferometry. Appl Opt. 1992; 31(31):6637-6642

Horio N, Kachi S, Horio K, Okamoto Y, Yamamoto E, Terasaki H: Progressive change of optical coherence tomography scans in retinal degeneration slow mice. Arch Ophthalmol 2001;119:1329-1332

Huang D, Swanson EA, Lin CP, Schuman JS, Stinson W, Chang W, Hee MR, Flotte T, Gregory K, Puliafito CA, Fujimoto JG: Optical Coherence Tomography. Science 1991; 254:1178-1181

Huang D, Wang J, Lin CP, Puliafito CA, Fujimoto JG: Micron-resolution ranging of cornea and anterior chamber by optical reflectometry. Lasers Surg Med. 1991; 11:419-425

Huang Y, Cideciyan AV, Papastergiou GI, Banin E, Semple-Rowland SL, Milam AH, Jacobsen SG: Relation of Optical Coherence Tomography to Microanatomy in Normal and *rd* Chickens. IOVS 1998; 39(12):2405-2416

Huber G, Beck SC, Grimm C, Sahaboglu–Tekgoz A, Paquet-Durand F, Wenzel A, Humphries P, Redmond TM, Seeliger MW, Fischer MD: Spectral domain optical coherence tomography in mouse models of retinal degeneration. IOVS 2009

I

Institute for Laboratory Animal Research (ILAR): Recognition and alleviation of pain and distress in laboratory animals. National Academy Press, Washington D.C., 1992

Izatt JA, Hee MR, Swanson EA, Lin CP, Huang D, Schumann JS, Puliafito CA, Fujimoto JG: Micrometer-scale resolution imaging of the anterior eye in vivo with optical coherence tomography. Arch Ophthalmol. 1994; 112(12): 1584-1589

K

Kaneko A: Physiology of the Retina. Ann. Rev. Neurosci. 1979; 2:169-91

Kellner U, Wachtlin J: Retina. 2008 Georg Thieme, Stuttgart

Kim K, Maguluri GN, Puoris'haag M, Umino Y, Barlow RB, de Boer JF:Optical Coherence Tomography for Mouse Retinal Imaging. Invest. Ophthalmol. Vis. Sci. 2006 47: E-Abstract 2923

Kim KH, Puoris`haag M, Maguluri GN, Umino Y, Cusato K, Barlow RB, de Boer JF: Monitoring mouse retinal degeneration with high-resolution spectral-domain optical coherence tomography. Journal of Vision 2008; 8(1):17, 1-11

Ko TH, Adler D, Fujimoto JG, Mamedov D, Prokhorov V, Shidlovski V, Yakubovich S: Ultrahigh resolution optical coherence tomography imaging with a broadband superluminescent diode light source. Opt Express 2004;12(10):2112-2119

Ko TH, Fujimoto JG, Duker JS, Paunescu LA, Drexler W, Baumal CR, Puliafito CA, Reichel E, Rogers AH, Schuman JS: Comparison of Ultrahigh and Standard Resolution Optical Coherence Tomography for Imaging Macular Hole Pathology and Repair. Ophthalmology 2004; 111:2033-2043

Kocaoglu OP, Uhlhorn SR, Hernandez E, Juarez RA, Will R, Parel JM, Manns F: Simultaneous Fundus Imaging and Optical Coherence Tomography of the Mouse Retina. IOVS 2007; 48(3):1283-1289

Kolb H, Fernandez E, Nelson R: The organization of the vertebrate retina. Available at http://webvision.med.utah.edu/ Accessed April 2002

L

LaVail MM, Yasumara D, Matthes MT: Protection of mouse photoreceptors by survival factors in retinal degenerations. IOVS 1998;39:592-602

Leitgeb R, Hitzenberger CK, Fercher AF: Performance of Fourier domain vs. time domain optical coherence tomography. Optics Express 2003; 11:889-894

Leitgeb RA: Optical coherence tomography – high resolution imaging of structure and function. Conf Proc IEEE Eng Med Biol Soc. 2007;2001:530-2

Lewin AS, Drenser KA, Hauswirth WW: Ribozyme rescue of photoreceptor cells in a transgenic rat model of autosomal dominant retinitis pigmentosa. Nat Med 1998; 4:967-971

Lhériteau E, Libeau L, Stieger K, Deschamps JY, Mendes-Madeira A, Provost N, Lemoine F, Mellersh C, Ellinwood NM, Cherel Y, Moullier P, Rolling F: The RPGRIP1-deficient dog, a promising canine model for gene therapy. Mol Vis 2009;15:349-61. Epub 2009 Feb 18.

Li Q, Timmers AM, Hunter K, Gonzalez-Pola C, Lewin AS, Reitze DH, Hauswirth WM: Noninvasive Imaging by Optical Coherence Tomography to Monitor Retinal Degeneration in the Mouse. IOVS 2001;42(12):2981-2989

Liew G, Wan JJ, Mitchell P, Wong TY: Retinal Vascular Imaging: A New Tool in Microvascular Disease Research. Circ Cardiovasc Imaging 2008;1:156-161

M

Marmor MF, Zrenner E: Standard for clinical electro-oculography. International Society for Clinical Electrophysiology of Vision. Arch Ophthalmol 1993 ; 5(111):601-4

Martinez-Morales JR, Rodrigo I, Bovolenta P: Eye development: a view from the retinal pigmented epithelium. BioEssays 2004; 26:766-777

Massin P, Allouch C, Haouchine B, Metge F, Paques M, Tangui L, Erginay A, Gaudric A: Optical coherence tomography of idiopathic macular epiretinal membranes before and after surgery. American Journal of Ophthalmology 2000; 130(6):732-739

Michaelson IC: The mode of development of the vascular system of the retina, with some observations on its significance for certain retinal diseases. Trans Ophthalmol. Soc. UK 1948; 68:137-181

Morton DB, Townsend P: Dealing with Adverse Effects and Suffering During Animal Research. Laboratory Animals - An Introduction for Experimenters 1995, 2nd Edn. (ed. A.A. Tuffery):215-231

N

Nassif N, Cense B, Park BH, Yun SH, Chen TC, Bouma BE: In vivo human retinal imaging by ultrahigh-speed spectral domain optical coherence tomography. Optics Letters 2004; 29:480-482

O

Ogden TE: Nerve fiber layer of the primate retina: thickness and glial content. Vision Res 1983; 23:581

P

Panzan CQ, Güven D, Weiland JD, Lakhanpal RR, Javaheri M, de Juan E Jr, Humayun MS: Retinal thickness in normal and rcd1 dogs using optical coherence tomography. Ophthalmic Surg Lasers Imaging 2004;35(6):485-93

Paques M, Simonutti M, Roux MJ, Picaud S, Levavasseur E, Bellmann C, Sahel JA: High resolution fundus imaging by confocal scanning laser ophthalmoscopy in the mouse. *Vision Res*. 2006;46:1336-1345

Petersen-Jones SM: Animal models of human retinal dystrophies. Eye 1998; 12:566-570

Pircher M, Gotzinger E, Leitgeb R, Sattmann H, Findl O, Hitzenberger CK: Imaging of polarization properties of human retina in vivo with phase contrast resolved transversal PS-OCT. Opt Express 2004; 12:5940-5951

Podoleanu AG, Dobre GM, Webb DJ, Jackson DA: Simultaneous en-face imaging of two layers in the human retina by low-coherence reflectometry. Opt Lett 1997; 22(13):1039-1041

Podoleanu AG, Dobre GM, Jackson DA: En-face coherence imaging using galvanometer scanner modulation. Opt Lett 1998; 23(3):147-149

Preece SJ, Claridge E: Monte Carlo modeling of the spectral reflectance of the human eye. Physics in Medicine ND Biology 2002; 47:2863-2877

Puliafito CA, Hee MR, Schuman JS, Fujimoto JG: Optical coherence tomography of ocular disease. 1995

R

Rattner A, Sun H, Nathans J: Molecular Genetics of Human Retinal Disease. Annu.Rev.Genet. 1999; 33:89-131

Richmond J: Refinement, Reduction, and Replacement of Animal Use for Regulatory Testing: Future Improvements and Implementation within the Regulatory Framework. ILAR Journal 2002; 43:63-68

Rodieck RW: The first steps in seeing. Sunderland, Mass 1998, Sinauer Associates

Rosen RB, Hathaway M, Rogers J, Pedro J, Garcia P, Dobre GM, Podoleanu AG: Simultaneous OCT/SLO/ICG Imaging. IOVS 2009; 50(2):851-860

Ruether K, van de Pol D, Jaissle G, Berger W, Tornow RP, Zrenner E: Retinochisislike alterations in the mouse eye caused by gene targeting of the Norrie disease gene. Invest Ophthalmol Vis Sci. 1997;38:710-718

Ruggeri M, Wehbe H, Jiao S, Gregori G, Jockovich ME, Hackam A, Duan Y, Puliafito CA: In vivo Three-Dimensional High-Resolution Imaging of Rodent Retina with Spectral-Domain Optical Coherence Tomography. Invest Ophthalmol Vis Sci. 2007; 48(4):1808-1814

Russel WMS and Burch RL: The Principles of Humane Experimental Technique. Methuen, London, 1959

S

Schuman JS, Hee MR, Puliafito CA, Wong C, Pedut-Kloizman T, Lin CP, Hertzmark E, Izatt JA, Swanson EA, Fujimoto JG: Quantification of nerve-fiber layer thickness in normal and glaucomatous eyes using optical coherence tomography-a pilot study. Arch Ophthalmol. 1995; 113(5):586-596

Schuman JS, Pedut-Kloizman T, Hertzmark E, Hee MR, Wilkins JR, Coker JG, Puliafito CA, Fujimoto JG, Swanson EA: Reproducibility of nerve fiber layer thickness measurements using optical coherence tomography. Ophthalmology 1996; 103(11):1889-1898

Schuman JS, Puliafito CA, Fujimoto JG: Optical coherence tomography of ocular disease. 2004

Seeliger MW, Beck SC, Pereyra-Munoz N, Dangel S, Tsai JY, Luhmann UFO, van de Pavert SA, Wijnholds J, Samardzija M, Wenzel A, Zrenner E, Narfström K, Fahl E, Tanimoto N, Acar N, Tonagel F: In vivo confocal imaging of the retina in animal models using scanning laser ophthalmoscopy. Vision Research 2005; 45:3512-3519

Seeliger MW, Grimm C, Ståhlberg F, Friedburg C, Jaissle G, Zrenner E, Guo H, Remé ChE, Humphries P, Hofmann F, Biel M, Fariss RN, Redmond TM, Wenzel A: New views on RPE65 deficiency: the rod system is the source of vision in a mouse model of Leber congenital amaurosis. Nat Genet 2001; 29: 70-74

Sharma RK, Ehinger BEJ. Development and Structure of the Retina. Adler`s Physiology of the Eye 2003, Chapter 10. Mosby, St. Louis, Missouri

Spalton DJ, Hitchings RA, Hunter PA: Atlas of clinical ophthalmology. Wolfe Publishing, London, UK. 1994(2nd edition), Chapter 11

Srinivasan VJ, Ko TH, Wojkowski M, Carvalho M, Clermont A, Bursell SE, Song QH, Lem J, Duker JS, Schuman JS, Fujimoto JG: Noninvasive Volumetric Imaging and Morphometry of the Rodent Retina with High-Speed, Ultrahigh-Resolution Optical Coherence Tomography. IOVS 2006; 47(12):5522-5528

Swanson EA, Huang D, Hee MR, Fujimoto JG, Lin CP, Puliafito CA: High-speed optical coherence domain reflectometry. Optics Letters 1992; 17:151-153).

Swanson EA, Izatt JA, Hee MR, Huang D, Lin CP, Schuman JS, Puliafito CA, Fujimoto JG: In vivo retinal imaging by optical coherence tomography. Optics Letters 1993; 18(21): 1864-1866

T

Takahashi JS, Pinto LH, Vitaterna MH: Forward and reverse genetic approaches to behaviour in the mouse. Science 1994; 264:1724-1733

Toth CA, Narayan DG, Boppart SA, Hee MR, Fujimoto JG, Birngruber R, Cain CP, DiCarlo CD, Roach WP: A comparison of retinal morphology viewed by optical coherence tomography and by light microscopy. Arch Ophthalmol. 1997; 115:1425-1428

W

Wässle H: Parallel processing in the mammalian retina. Nat Rev Neurosci 2004;5(10):747-57

Wojtkowski M, Bajraszewski T, Gorczynska I, Targowski P, Kowalczyk A, Wasilewski W, Radzewicz C: Ophthalmic Imaging by Spectral Optical Coherence Tomography. Am J Opth 2004; 138:412-419

Wojtkowski M, Srinivasan V, Ko T, Fujimoto J, Kowalczyk A, Duker J: Ultrahigh-resolution, high-speed, Fourier domain optical coherence tomography and methods for dispersion compensation. Opt Express 2004;12(11):2404-2422

Wolf – Schnurrbusch UE, Enzmann V, Brinkmann CK, Wolf S: Morphological changes in patients with geographic atrophy assessed with a novel spectral OCT-SLO combination. Invest Ophthalmol Vis Sci. 2008;49:3095-3099

Wu SM, Baehr W, Crair M: The mouse visual system: from photoreceptors to cortex. Vis Res 2004;44:3233-3234

X

Xu H, Manivannan A, Goatman KA, Liversidge J, Sharp PF, Forrester JV, Crane IJ: Improved leukocyte tracking in mouse retinal and choroidal circulation. Exp Eye Res. 2002;74:403-410

Xu Q, Wang Y, Dabdoub A, Smallwood PM, Williams J, Woods C, Kelley MW, Jiang L, Tasman W, Zhang K, Nathan J: Vascular development in the retina and inner ear: control by Norrin and Frizzled-4, a high-affinity ligand-receptor pair. Cell 2004;116:883-895

Y

Yazdanfar S, Rollins AM, Izatt JA: In vivo imaging of human retinal flow dynamics by color Doppler optical coherence tomography. Arch Ophthalmol. 2003; 121:235-239

IX. ACKNOWLEDGEMENTS

Mein Dank gilt Herrn Prof. Dr. Dr. M. Erhard für die Übernahme meiner Arbeit, deren Durchsicht und Einreichung an der tierärztlichen Fakultät der Ludwigs-Maximilians-Universität.

Ich danke Herrn Prof. Dr. M. Seeliger für die Möglichkeit der Durchführung dieser Arbeit in seinem Labor, für seine Unterstützung sowie für die kritische Durchsicht der Manuskripte und der Arbeit.

Bei Herrn Dr. F. Iglauer möchte ich mich für die Unterstützung bei der Anfertigung dieser Arbeit und bei allen tiermedizinischen Fragestellungen meiner Tätigkeit bedanken.

Ich danke der Kerstan Foundation für die finanzielle Unterstützung.

Mein besonderer Dank gilt Frau Hofer für all ihre graphischen Meisterleistungen.

Herrn Adler möchte ich für seinen freundlichen „Bereitschaftsdienst“ bei wiederholten EDV-Problemen danken.

Ein herzliches Dankeschön an meine Kollegen Susanne Beck, Edda Fahl, Regine Mühlfriedel, Naoyuki Tanimoto, Gudrun Utz sowie Dominik Fischer für die fachkundige und stetige Hilfestellung und die netten Stunden im Labor und drum herum.

Für die mentale Unterstützung und den Rückhalt während dieser Zeit möchte ich mich im Besonderen bei Björn Beck bedanken.

Meinen Eltern und vor allem meinem Bruder Felix ein herzliches Dankeschön für ihre stetige Unterstützung in allen Belangen und das umfassende „humane treatment“.